NTNU
Norwegian University of
Science and Technology

Effects of Shading on PV Power Production in Norwegian Climates

Carolyn Marie Willems

Innovative Sustainable Energy Engineering
Submission date: June 2018
Supervisor: Eivind Øvrelid, IMA
Co-supervisor: Marisa Di Sabatino Lundberg, IMA

Norwegian University of Science and Technology
Department of Materials Science and Engineering

Effects of Shading on PV Power Production in Norwegian Climates

Preface

This thesis is delivered in partial fulfillment of a Joint Nordic MSc. in Innovative Sustainable Energy Engineering. It was carried out in the spring semester of 2018 at NTNU in The Department of Material Science and Engineering, in collaboration with the Sustainable Energy Technology department at SINTEF. The body of work corresponds to 30 ECTS. It was supervised by Eivind Johannes Øvrelid and Marisa Di Sabatino Lundberg from NTNU. The co-supervisor from the Nordic Five Tech. partner university was Sune Thorsteinsson from DTU.

This Master's thesis builds upon the work done in the fall semester of 2017 as part of a specialization project corresponding to 15 ECTS. Overlapping content has been amended accordingly.

June 2018
Trondheim, Norway

Carolyn Willems

Acknowledgements

This thesis would not have been possible without the help and support of many.

First of all, I would like to thank my supervisor from NTNU, Eivind Johannes Øvrelid, for your excellent guidance and dedication throughout this semester. I would also like to thank my co-supervisor from NTNU, Marisa di Sabatino Lundberg for your encouragement and support all the way from France. Further, I want to thank Sune Thorsteinsson, my DTU supervisor along with his team Nicholas Riedel and Jørgen Schou for always being available for Skype calls and providing enriching insight into the project.

I want to sincerely thank Gaute Stokkan from SINTEF. All of your hard work did not go unnoticed and this thesis would not be possible without the countless hours you spent building and upkeeping the test site.

A special thank you to Øystein Holm and Anna Frederikke Østby from Multiconsult for all of your hard work setting up the shading elements on the roof system and your contribution with data collection. Your constant interest and enthusiasm in the project was greatly appreciated.

Thank you to my fellow ISEE students Kevin, Annika, Johanna and honorary member Matt. Our monthly meetings kept me motivated up until the very end.
A special thank you to my Canadian and Norwegian family for your generous encouragement and support. Lastly, I would like to thank Emil Anthonsen Dyrstad for your instant responses to my questions about electricity and your unwavering support through out these past 3 years.

Abstract

Policy, and a significant decrease in cost have played a major role in bringing photovoltaic solar to the forefront as a renewable energy source and a lucrative business opportunity around the world. The Norwegian solar industry is continually increasing however, due to a variability in weather patterns and a lack of accurate data, PV output predictions in Norway have proven to be less accurate than in other parts of the world where the PV industry is more established. This Master's thesis aims to provide insight into improving models, predictions and the future planning of PV systems in Norway and areas of similar climate.

The goal of this thesis is to analyze two small scale PV systems in Norway to understand the role that snow and partial shading play in the overall energy output of a system. First, a small scale building integrated system is modelled in a PV modelling software to provide a benchmark in which to compare the measured energy output. The snow coverage of the system was calculated by performing image analysis on timelapse images taken of the system and compared to the measured energy output. To understand partial shading at a system level, three shading scenarios were carried out on a small scale roof top building in Skøyen, Norway, utilizing three types of inverter technologies. Energy output values from the shading scenarios were then implemented into an economic analysis to compare levelized costs for each technology.

This project has shown that an average daily reduction in energy output of 11 % can be measured when snow and ice is present on a PV system in Nordic climates, however, the overall effect of snow on a system may be balanced by the increased diffuse irradiation when snow is present around the PV system but not covering the modules. An economic analysis of a test site in Skøyen determined that micro inverters presented the lowest levelized cost when no shading was imposed on the system, followed by DC optimizers.

Sammendrag

Støtteordninger, sammen med en markant reduksjon i kostnader har vært svært viktig for å få fotovoltaisk solenergi frem som en av de viktigste kildene til fornybar energi og som en lukrativ forretningsmulighet. Den norske solindustrien blir stadig større, men grunnet mangel på nøyaktige modeller for potensialet til solceller, har industrien fortsatt store muligheter. Denne masteroppgaven har som mål i gi innsikt i arbeidet med å forbedre modeller og analyser av PV-systemer i Norge og områder med lignende klima.

Målet med oppgaven er å observere to småskala PV-systemer i Norge, for å kunne bedre forståelsen av påvirkningen snø og annen delvis skyggelegging har på den totale energiproduksjonen. Første delen av oppgaven inkluderer modellering av ett bygningsintegrert PV-system ved hjelp av egnet programvare. Dette ble gjort som en målestokk for å kunne sammenligne målte energiproduksjoner. Systemets snødekning ble beregnet ved å utføre bildeanalyse av bilder tatt med jevne mellomrom. Disse resultatene ble sammenlignet med de målte energiutbyttene. For å vise effekten av delvis skyggelegging på systemnivå ble det utført flere forsøk på ett småskala PV-system installert på taket av en bygning på Skøyen, Oslo. Her ble det også brukt tre forskjellige omformere, for å kunne sammenligne betydningen de forskjellige teknologiene har. Energiproduksjonen fra de forskjellige scenarioene ble videre brukt i en økonomisk analyse. Den viste at mikroomformere var mest lønnsom.

Oppgaven har vist at snø og is på solcellesystemer i nordisk klima kan føre til en gjennomsnittlig reduksjon i energiproduksjonen på ca. 11 %. Noe av dette tapet vil likevel gjøres opp pga. den økte diffuse strålingen som snø på omgivelsene vil medføre.

Contents

List of Figures

List of Tables

Chapter 1

Introduction

According to the Intergovernmental Panel on Climate Change (IPCC), the electricity and heat sector accounts for 25 % of global greenhouse gas emissions [1]. As the Earth continues to experience the effects of anthropogenic climate change, there is a pressing need to decarbonize the energy sector and mitigate these effects. Policy, and a significant decrease in cost played a major role in bringing photovoltaic (PV) solar to the forefront as a renewable energy source and a lucrative business opportunity around the world.

World Energy Outlook

Currently, the energy sector accounts for approximately 60 % of total global greenhouse gas emissions [1]. The IPCC states that "human influence on the climate system is clear, and recent anthropogenic emissions of greenhouse gases are the highest in history. Recent climate changes have had widespread impacts on human and natural systems" [1]. Simultaneously, an increasing amount of the world's population is gaining access to electricity.

A recent report by DNV GL, *The Energy Transition Outlook*, therefore states that the global energy transition has two main characteristics moving forward: 1) decarbonization of the energy sector and 2) global electrification. If the energy sector continues to rely on fossil fuel based energy technologies, these two main characteristics will fail to converge [2].

United Nations Sustainable Development Goals

The future of energy cannot be discussed without mentioning the UN's Sustainable Development Goals - 17 goals with 169 targets to be achieved by 2030. These goals were adopted in September 2015 by 194 countries, including all Nordic countries. Specifically, Goal 7: "Ensure access to affordable, reliable, sustainable and modern energy for all," addresses the energy needs of the future. One of the targets of Goal 7 set by the Sustainable Development Goals working group is to substantially increase the share of renewable energy in the global energy mix by 2030 [3]. These goals and targets have informed many of the new policies and regulations set by the EU/EEA. For example, Norway has committed to reduce their emission by

40 % compared to 1990 levels by 2030 [4]. To help reach this goal, the EU/EEA has declared that all new buildings built after 2020 must be "nearly Zero Energy Buildings" [5]. In order to achieve this target, buildings must be designed to be highly energy efficient, and any additional energy needs must therefore be produced locally. Therefore, PV technology is and will increasingly become a crucial step towards the decarbonization of the electricity sector.

Norway's Current Electricity System

Norway has a long history as an energy powerhouse within the EU. As one of the largest oil and gas exporters in the world and one of the most significant energy producers and exporters in Europe. Norway produces on average 130 TWh of electricity yearly, with 96 % coming from renewable hydro power. The 85 TWh in hydropower storage capacity provides balancing power to neighbouring countries. In 2015, 14.8 TWh (11.4 %) was exported to neighbouring countries including Sweden, Denmark, and the Netherlands [6]. The interest within Europe to gain access to Norway's clean, reliable and affordable electricity is further exemplified by the addition of two interconnectors which are currently in the construction phase: the NordLink HVDC cable is expected to connect Germany to the Norwegian grid by 2020 [7, 8], and the North Sea Link (NSL) interconnector is expected to link British and Nordic markets by 2021 [9].

Hydropower is a great source of baseload electricity, while solar power provides electricity during peak times when possible, making them complimentary energy sources. Introducing more solar into the electricity mix increases Norway's capacity of providing renewable energy to neighbouring countries that may be struggling to meet their energy demand at certain times or who still have a large percentage of fossil fuel based electricity in their energy mix.

Development of PV in Norway

Norway has seen its fair share of development in the PV industry over the last decade. Due to relatively cheap electricity prices, Norway has been producing ferro-silicon for many years, and in recent years has established itself as a producer of solar-grade silicon [10].

In terms of PV planning, engineering, and installation in Norway, the industry is relatively small and recent, but steadily growing. According to a preliminary International Energy Agency (IEA) report from 2016, the five largest installations in the country are grid connected with the largest three having a capacity of over 1 MW. The market also showed strong growth from 2015 to 2016 when it was

confirmed by the Norwegian Parliament that solar PV installations would be eligible for green electricity certificates [11]. It is estimated that over 42 MW of solar will have been installed by the end of 2017 [11]. Figure 1.1 shows the increase in PV installations from 2011 to 2017.

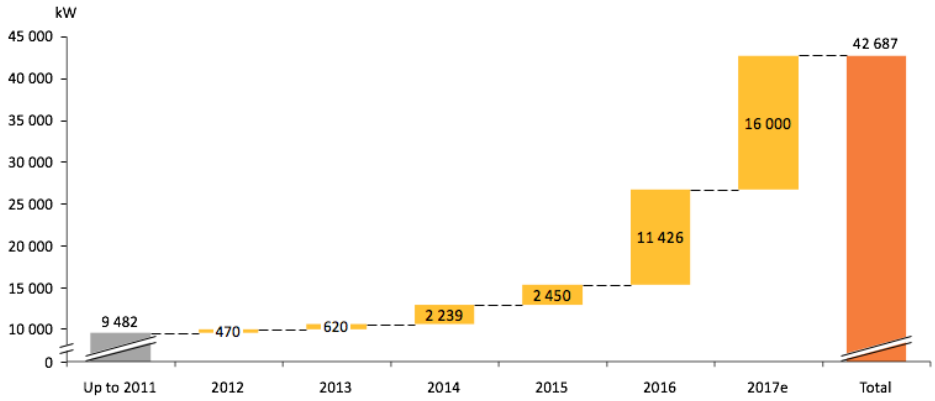

Figure 1.1: PV installation capacity from 2011-2017 (expected) [11].

The cost of solar PV continues to decline at an exponential rate [12], and an increasing number of businesses are being developed in Norway to meet the increasing demand for PV in Norway. However, the industry faces many challenges ahead. Due to a variability in weather patterns and a lack of accurate data, PV output predictions in Norway have proven to be less accurate than in other parts of the world where the PV industry is more established. A greater challenge is presented when considering PV generation under snow covered conditions.

Therefore, this work aims to offer results which can aid to improve models, predictions and the future planning of PV systems in Norway and areas of similar climate.

1.1 Objectives

The underlying objectives of this thesis are to identify how Norwegian climates affect PV power production and how these effects can be taken into account when planning such systems. In order to fulfill this objective, the following tasks were a part of this thesis:

1. Present the rudimentary theory on relevant PV technology.

2. Summarize the current research on cold climate PV systems, including soiling

due to snow.

3. Model a residential PV system in PV*Sol based on actual system characteristics.

4. Measure and monitor the snow coverage and system energy output of a residential PV system.

5. Perform an economic case study to compare the economic feasibility of inverter technologies under partial shading conditions.

1.2 Structure

The structure of this thesis is as follows:

- Chapter 1 gives an introduction to the topic of PV as a source of clean electricity. The objectives and structure of the report are also outlined.
- Chapter 2 outlines the current technology surrounding PV power systems.
- Chapter 3 presents the State of the Art regarding PV energy production under partial shading and in cold-climate regions.
- Chapter 4 outlines the residential PV system modelled in PV*Sol and the expected energy production. The instrumentation and methods are also introduced.
- Chapter 5 presents the results from the residential PV test site.
- Chapter 6 contains an economic assessment of a case study comparing string and micro inverters to combat partial shading.
- Chapter 7 provides a discussion on the preceding chapters.
- Chapter 8 presents conclusions based on the work and discusses important areas for further study.

Chapter 2

Basic Theory

The following chapter is meant to give a basic understanding of PV technology including how solar energy is generated, evaluated, and predicted.

2.1 Current PV Technology

The PV cell industry is continually working to achieve cells with higher efficiencies that are easier and cheaper to produce. Currently, there are three main technologies that make up the market: 1) mutli-crystalline silicon (multi-Si), 2) mono-crystalline silicon (mono-Si), and 3) thin films. It is estimated that around 75 GW_p of PV modules were produced in 2016 with 69 % being multi-Si, 24 % being mono-Si, and 6 % being thin films [13].

Mono-Si and multi-Si are also known as first generation technologies and rely on single junction wafers, meaning that they contain a single layer of light absorbing material. According to the most recent solar cell efficiency tables by Green et al. [14], these cells have reached a record efficiency of 26.3 % $\pm$ 0.5 % and 21.3 % $\pm$ 0.4 %, respectively. Some of the success of first generation solar cells can be attributed to the fact that the industry grew alongside the integrated circuit industry, therefore providing greater access to processing and manufacturing techniques, and large scale production [15].

Second generation PV cells are also single junction devices but were designed to use less materials therefore lowering costs. These types of solar cells are often referred to as thin film solar cells since they are made by depositing thin layers onto a substrate. Materials used in these types of cells are amorphous silicon (a-Si), CIS, and CdTe. These materials are able to absorb the solar spectrum more efficiently, while using much less material. According to the most recent solar cell efficiency tables by Green et al. [14], a-Si cells have reached an efficiency of 10.5 % $\pm$ 0.3 % whereas CIS and CdTe cells have reached up to 21 % efficiency. The main setback with second generation cells has been difficulties in scaling up the technology as well as poor reproducibility.

Third generation solar cells are currently of great interest, but still have a long way to go before they are able to be produced cheaply and with a reasonable lifetime. As first generation cells are reaching their maximum theoretical efficiency

of 34 % based on the Shockley–Queisser (SQ) limit, third generation cells are able to improve on that limit by having multiple junctions which perform at different band gap energies. Examples of these emerging technologies are multiple band gap solar cells, intermediate band gap solar cells, dye-sensitized solar cells (DSSC) and quantum dot cells. Perovskite cells have been able to reach up to 19.7 % ± 0.6 % efficiency but the cells lose a significant portion of their efficiency in a relatively short time [14].

2.2 The Silicon Solar Cell

Silicon solar cells are by far the most widely used technology in the PV industry to date, at an estimated 93 % [15]. The following sections will therefore explain the physics of PV from the perspective of crystalline solar cells.

A PV cell is an electronic device used to convert the light energy in the form of photons into electricity. In simple terms, the cell is fabricated with a positive (p-type) and negative (n-type) layer by adding doping elements, creating a positive-negative junction junction where the two layers meet. To understand what is happening at the p-n junction of a cell, three basic principals are described:

1. The establishment of a depletion zone at the junction.
2. Absorption of light generating electron-hole pairs.
3. The directional extraction of free charge carriers.

The negatively charged layer contains an excess of electrons whereas the positively charged layer contains atoms with electron holes. These are known as charge carriers because they are free to roam around within the material. When the n-type and p-type layers are connected, the negative charge carriers (electrons) and positive charge carriers (holes) diffuse into the opposite sides of the junction, creating a depletion zone. The separated positive and negative chargers at the junction create an electric field across the depletion zone.

When the cell is illuminated, the interaction between the incident photons from the light source and atoms of the cell generate more electron hole pairs, or free charge carriers. The electric field that had already been established at the junction encourages the free charge carriers (electrons) to flow in the opposite direction of the electric field. This flow of electron creates a direct current which is collected through cell terminals. This process can be seen in Figure 2.1 [16].

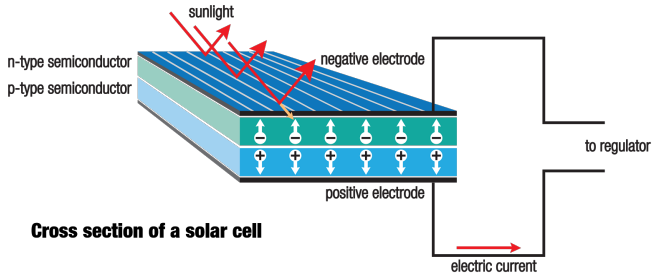

Figure 2.1: Cross section of a PV solar cell [17].

2.3 PV Characteristics

Based on the governing principals of the p-n junction, a standard solar cell can be described electrically as a diode and a current source connected in parallel as shown in the following ideal equivalent circuit diagram (Figure 2.2). The diode is formed by the p-n junction in the cell. When the cell is in dark state, it acts as a characteristic diode. As mentioned in Section 2.2 when a PV cell is illuminated, free charge carriers are created and current flows through a connected load. The number of free charge carriers is proportional to the incident radiation intensity from the light. I_l is then the current generated in the cell form illumination. This produces a voltage across the diode (V_D), corresponding to the current generated in the diode (I_D) [16].

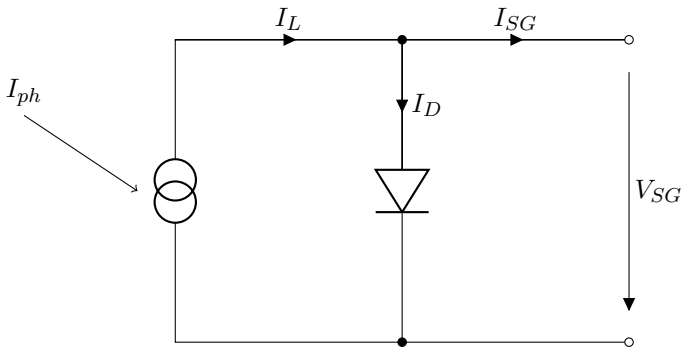

Figure 2.2: Equivalent circuit for an ideal solar cell where SG stands for solar generation. Schematic adapted from [18].

For an ideal cell, the IV curve can be described by the following characteristic equation:

$$I = I_o\left(e^{\frac{V_A}{V_T}} - 1\right) \tag{2.1}$$

Where I_0 is the diode saturation current at the applied voltage, V_A. V_T is the thermal voltage which is constant, and I_L is the light generated current [18].

When the junction is illuminated, a light generated current (I_L) is also added as seen in Equation 2.2. The negative sign is due to polarity conventions.

$$I = I_o\left(e^{\frac{V_A}{V_T}} - 1\right) - I_L \tag{2.2}$$

For a more accurate description of the PV cell, two additional resistances must be included into the ideal equivalent circuit diagram (Fig. 2.2) to represent the losses that occur in the cell. The R_s is the resistance through the silicon wafer as well as all electrical contacts, connections and terminals in the cell. The shunt resistance (R_{sh}) is the loss at the edges of the cell and surface inhomogeneities. A more realistic equivalent circuit diagram is illustrated in Figure 2.3.

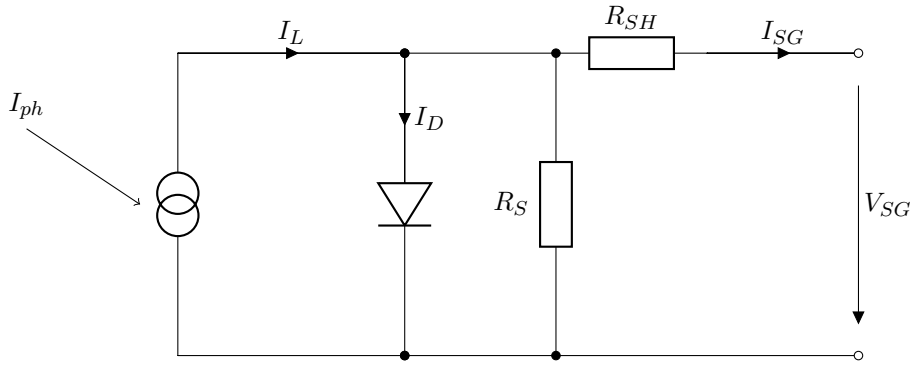

Figure 2.3: Equivalent circuit diagram for a crystalline silicon solar cell including R_{SH} and R_S where SG stands for solar generation. Schematic adapted from [18].

These characteristic equations can be plotted to form a characteristic IV curve as illustrated in Figure 2.4. The main characteristics as illustrated in Figure 2.4 and described below are: 1) I_{sc}, 2) V_{oc}, 3) maximum power point (MPP) 4) fill factor, and 5) [16]. It should be noted that the curve is often depicted to reflect Equation 2.2 such that the curves are mirrored in the x-axis. Conventional logic dictates that the MPP is expected to appear in the first quadrant, and it is often flipped as shown in Figure 2.4.

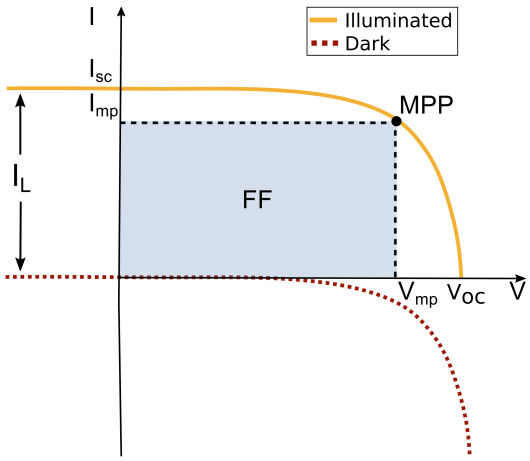

Figure 2.4: IV characteristics of a solar cell in dark state and illuminated. Adapted from [19].

Short Circuit Current

The I_{sc} is the current that flows through the circuit when the electrodes of the solar cell have been short circuited. I_{sc} is dependant on the incident photon flux on the cell determined from the spectrum of the incident light and the temperature of the cell, which is further discussed in Section 2.5.3. Other factors affecting I_{sc} are the optical properties of the cell such as reflection and the absorption in the absorbing layer [16].

Open Circuit Voltage

The V_{oc} is the voltage of the cell when no current is flowing through the circuit. As can be seen from Figure 2.4, it is the maximum possible voltage that a solar cell can deliver. The V_{oc} is dependant on the saturation current density and the photo-generated current. Contrary to the I_{sc}, V_{oc} is negatively effected by an increase in temperature [16]. The cell's relationship to temperature will be discussed further in Section 2.7.

Maximum Power Point

The MPP of the cell is the point on the IV curve where the solar cell has the maximum power output. While it is the product of I_{sc} and V_{oc}, the resistance in the cell make the IV curve less rectangular, therefore reducing the maximum power output. To achieve the optimum output of the cell, it must be operated

at the MPP at all times. In practice, a maximum power point tracker (MPPT) is used to mathematically determine the optimal point of the cell or module, therefore achieving maximum output [16].

Fill Factor

The FF is the ratio between the maximum power generated by the cell and the product of the V_{oc} and I_{sc}. It can be described by the following equation:

$$FF = \frac{I_{mpp}V_{mpp}}{I_{sc}V_{oc}} \tag{2.3}$$

Where I_{mpp} and I_{mpp} are the current and voltage at the MPP. The FF describes how closely the IV characteristic is to the ideal rectangle form in Figure 2.4 [16]. The FF for c-Si solar cells is typically around 0.7–0.8 [18].

Efficiency

In simple terms, the efficiency is the percentage of power that is converted from absorbed light to electrical energy. It can be described as the ratio of the maximum generated power over the incident power of the cell as seen in Equation 2.4.

$$\eta = \frac{J_{sc}V_{oc}FF}{P_s} \tag{2.4}$$

Where P_s is the incident light power density [16]. Typical efficiencies of different PV technologies were discussed in Section 2.1.

2.4 PV Modules

Once PV cells are fabricated, they are electrically connected to form a module. The cells are typically connected in series which dictates that the total voltage of the module will be the sum of the voltages across each cell. Therefore, the current is constant and determined by the photocurrent produced in each cell. By connecting the cells in series, the module can produce more significant voltages, and therefore power levels. Figure 2.5a shows a schematic of how the cells of a module are connected in series.

A disadvantage to connecting the cells in series is that all cells are limited by the cell that generates the lowest current. If a cell produces at a lower current due to shading or defects, assuming all cells have a constant load, the voltage will drop across the module to account for the low current. However, the fully functioning cells will then compensate by producing high voltages and act as a reverse bias source on the faulty cells. The faulty cells will not be producing power and will

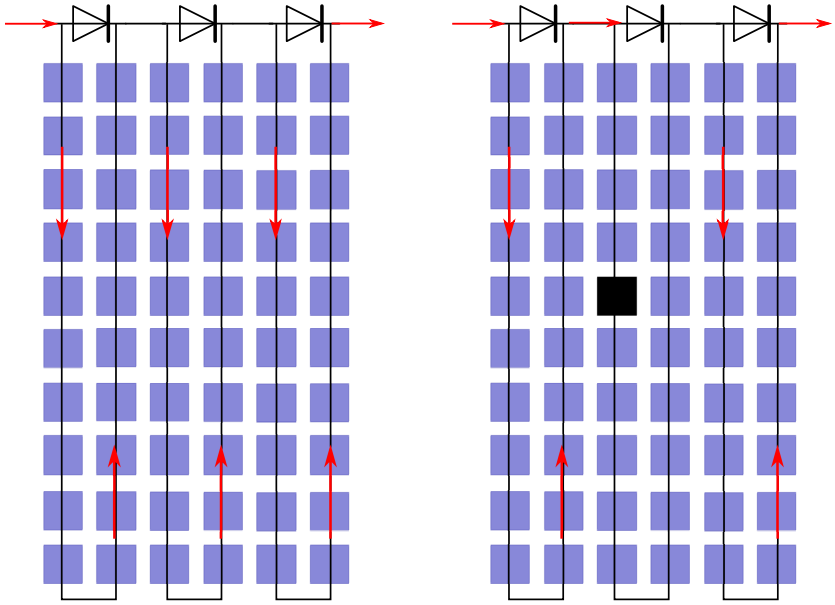

(a) The direction of current in a module when a cell is shaded and the bypass diode is activated.

(b) The direction of current in a module when a cell is shaded and the bypass diode is activated.

Figure 2.5: A schematic of a module showing the direction of current under normal and shaded conditions. Under a series configuration the current is constant and the voltage of the module is the sum of the voltage across each cell.

start to dissipate energy and therefore heat up. This concept is known as hot spots and can lead to damage in the module as well as significant losses in production.

In order to mitigate these effects, bypass diodes are installed in the module. These components work to bypass faulty cells and allows the module to continue producing current at the level of the properly functioning cells [20]. Figure 2.5b shows a schematic of how bypass diodes are used to bypass the shaded area of a module.

A standard PV module consists of the series connected cells which are sandwiched between plates of encapsulate, commonly EVA. Glass plates are put on both sides of the EVA and everything is encased in an aluminum frame. These modules are typically combined in groups of four to form a panel. A group of modules or panels in series is known as a string, where as a group of modules or panels in parallel is known as a solar array. A comparison of PV cells, modules and arrays is illustrated in Figure 2.6.

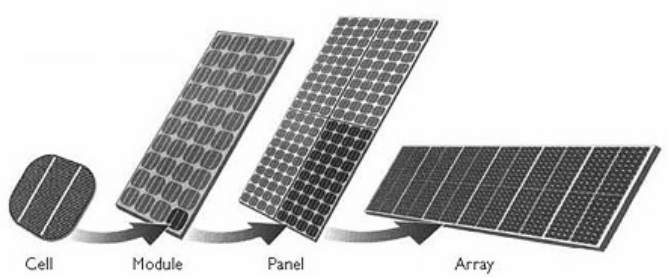

Figure 2.6: Components of a PV array [21].

2.4.1 System Configuration

A crucial component to a PV system is the electrical equipment needed to regulate and transmit the electrical power converted in the PV system. The following image illustrates the main components of a typical grid connected PV system without storage:

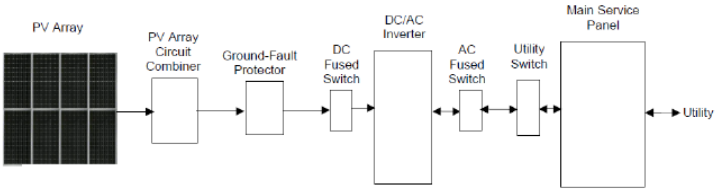

Figure 2.7: Schematic of the main electrical components and system configuration in a grid connected PV system without storage capacity [22].

The PV array combiner simply combines the electricity from each array and passes it through the ground-fault protector. The DC and AC fused switches are placed on either side of the inverter as a safety mechanism. The electricity is then passed through the utility switch and into the main service panel. For an off-grid system, a controller would be added after the PV array to determine weather the energy should be stored or sent directly to the DC load.

In the case of a grid connected system, the direct current (DC) must be converted into alternating current (AC) so that it can be accommodated by the grid. This is done using an inverter. Typically, standard string inverters are used in Norway. The string inverter determines the MPP of the string and converts it to AC. However, micro inverters and DC optimizers have been gaining popularity. Whereas string inverters are more suited for systems with similar sized modules and little to none shading, micro inverters convert the power directly at each

module. Therefore each module is not affected by the rest of the system. In general, inverters have an efficiency of around 95 %, however the efficiency may vary depending on the cell parameters [22].

PV Systems

In general, PV systems can be divided into three main categories:

Residential Scale	1 – 10 kW
Commercial Scale	10 – 1 MW
Utility Scale	$>$ 1 MW

This thesis will be analyzing test sites that are in the scale of residential PV systems [12].

2.5 External Performance Factors

Aside from the main characteristics of PV solar cells, external factors ultimately determine the energy output of the modules. The solar spectrum and irradiance, cell temperature, and shading effects are all factors that affect PV performance and should be considered when designing a system.

2.5.1 The Solar Irradiance and Spectrum

Irradiance is the measurement of the instantaneous power density of sunlight received at a certain location over a certain area. It is measured in $\mathrm{W/m^2}$. An increase in solar irradiance causes more photons to reach the cell, increasing both V_{oc} and I_{sc} and therefore PP. The general effect of irradiance on the I-V curve can be seen in Figure 2.10a where an increase in solar irradiance corresponds to an increase in yield [23].

The total amount of solar radiation at normal incidence at the top of the earth's atmosphere is known as the TSI or extraterrestrial solar irradiance. Of course, not all of this solar irradiance penetrates the atmosphere and reaches the earth's surface. Part of it is scattered or absorbed by particles in the atmosphere such as ozone, water vapour, aerosol, and clouds. As solar radiation traverses the earth's atmosphere it is redistributed into three main components as described in Equation 2.5.

G_d	The component of solar irradiation that arrives on the ground, directly in line from the sun.

G_{diff}	The component of solar irradiation that interacts with clouds and various particles.
G_r	The component of irradiation that is reflected off of non-atmospheric objects such as asphalt. This component is typically very small compared to the direct and diffuse radiation and rarely accounts for a significant portion of the irradiance experienced by PV modules.

G_g is therefore equal to the sum of the three components: G_d, G_{diff} and G_r, as illustrated in Equation 2.5 [23].

$$G_g = G_d + G_{diff} + G_r \tag{2.5}$$

Typically, weather stations measure solar irradiance on the horizontal plane. However, most PV modules are tilted to form a 90° angle with the sun during the day and maximize the amount of direct radiation. Since diffused radiation is equally distributed through out the sky, diffuse radiation is maximized when the panels are horizontal. Therefore, the higher the tilt angle, the less diffuse radiation will reach the panels. Typically, modules in Norway should be tilted between 30–40°C to receive maximum radiation [24, 25, 26].

While solar irradiance is the instantaneous measurement of solar power over an area, insolation is a measurement of the cumulative energy over an area for a defined amount of time. Figure 2.8 illustrates the daily average insolation in Norway in January and July. As can be seen from the image, a major challenge in Norway is the large variations from summer to winter months. For example, a clear summer day can yield up to 8500 $\mathrm{W/m^2}$ compared to a cloudy winter day which could yield only 20 $\mathrm{W/m^2}$.

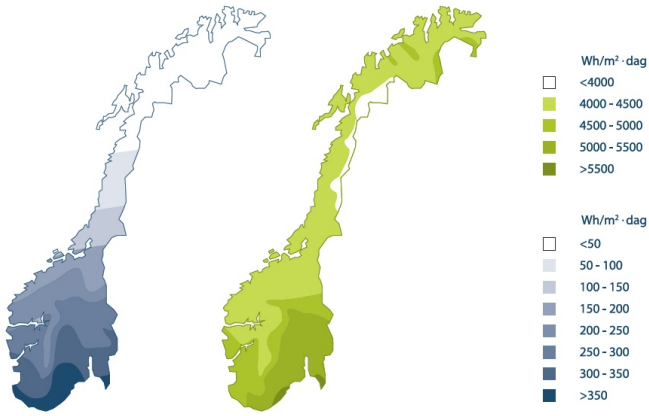

Figure 2.8: Average daily solar energy in Norway received by a horizontal surface in summer (left) and winter (right) [27].

2.5.2 Influence of Atmosphere

The air mass coefficient (AM) is a measurement describes the relative path of the direct solar radiance through the atmosphere. When the sun is directly overhead (also known as Zenith), the path length is 1.0, and experiences an AM of 1.0. Most locations on the earth do not have the sun directly at Zenith at solar noon, and it is therefore standard to consider when the sun is at a certain angle from the Zenith. When the angle from the Zenith increases, so does the AM. At about 48°, the AM is 1.5. A schematic and comparison of the different AM coefficients can be seen in Figure 2.9 [28].

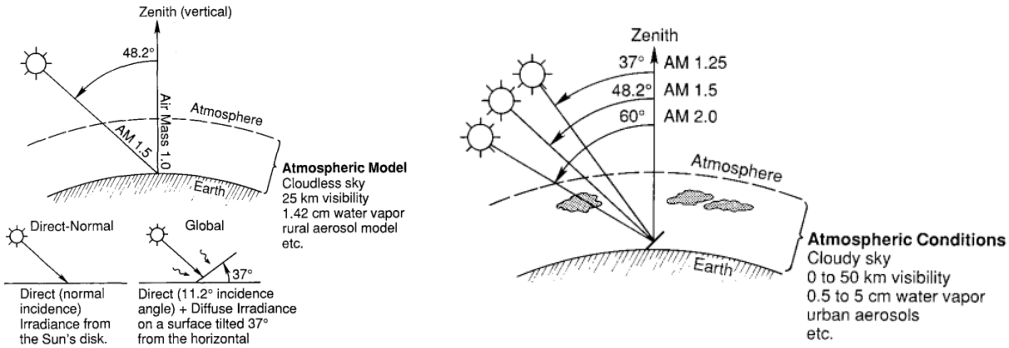

(a) Schematic of AM 1.5 conditions. (b) Comparison of different AM conditions.

Figure 2.9: Schematic of AM 1.5 spectrum conditions [28].

2.5.3 Temperature

It is well documented and known that an increase in the cell temperature (T_c) decreases the efficiency [29]. As the temperature increases, the band gap of the semiconductor decreases, therefore decreasing V_{oc}. Since the MPP is dependant on V_{oc}, a decrease will also decrease the MPP and therefore the efficiency of the cell [29]. It is important to note that I_{sc} increases slightly with temperature, but is over taken by the larger reductions in V_{oc}. The effect of temperature on a cell can be described by Equation 2.7

$$\eta = \eta_{T_{ref}}[1 - \beta_{ref}(T_c - T_{ref}) + \gamma log_{10} I(t)] \tag{2.6}$$

Where η_{ref} is the module's electrical efficiency at the reference temperature (T_{ref}) and at a solar radiation of 1000 W/m^2. The temperature coefficient (β_{ref}) and the solar radiation coefficient (γ) are material properties. For crystalline silicon cells, γ is typically assumed to be zero, therefore reducing the equation to a linear expression [30]:

$$\eta = \eta_{T_{ref}}[1 - \beta_{ref}(T_c - T_{ref})] \tag{2.7}$$

The general effect of temperature and irradiantion on the I-V curve can be seen in Figure 2.10b.

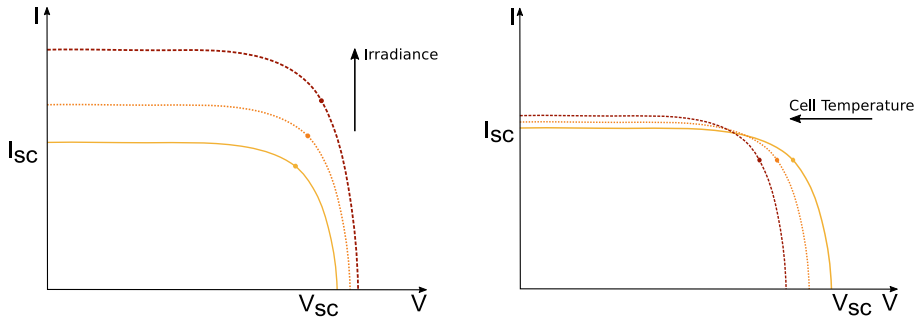

(a) Effect of irradiance.

(b) Effect of temperature.

Figure 2.10: Effect of irradiance and temperature on the I-V curve and subsequent MPP (shown as dot). Adapted from [30].

2.5.4 Standard Test Conditions

As the aforementioned external performance factors greatly effect the overall efficiency and output of the cell, standard test conditions (STC) have been

developed for industry to reliably compare all PV characteristics. All PV cells and modules are measured at a total irradiance of 1000 W/m^2, temperature of 25°C, and the spectrum must resemble AM1.5 [16]. By testing under STC, it is possible to compare different technologies.

Chapter 3

State of the Art

The following chapter describes the current body of research pertaining to PV energy production in cold-climate regions. Specifically, the influence that snow and ice have on obstruction of solar radiation is discussed, as well as the effects of partial shading on energy production.

3.1 PV Generation in Cold Climates

To date, over two-thirds of total PV resources have been installed in countries that experience a regular snowfall [31, 32]. Although much progress has been made, there is a continued need to investigate and understand how cold climate characteristics, including snow, affect the overall energy output of such systems. As previously mentioned, snow contributes to reductions in energy production due to full and partial shading.

Furthermore, the influence of snow and ice on PV energy output adds a layer of complexity to PV energy predictions due to the large variation in weather conditions and consequential snow formations. Current literature provides some insight into observed effects of soiling due to snow and ice as well as quantitative and qualitative analysis of snow formation on PV systems. Although little research has been performed to study the effect that snow has on PV performance in Norway, literature from similar climates will be compared to the results in the thesis in subsequent chapters.

3.1.1 The Characterization of Snow

In general, precipitation can be categorized into three types: rain, freezing rain or snow. Despite the fact that rain clouds block direct irradiation from the sun, rain itself is relatively harmless and in many cases helps to clean the modules of potential soiling such as dirt, dust, and bird droppings[33]. Freezing rain occurs when water droplets drop onto a surface that is below the freezing temperature and are supercooled, forming a layer of ice on the surface. Aside from having higher reflectivity properties than the AR coating on modules and inhibiting light absorption, ice is not inherently detrimental to PV production since it's visually transparent. However, snow can easily adhere to ice layers forming a coating of

snow and ice that is difficult to remove [34].

3.1.2 Optical Properties of Snow

The optical properties of snow vary based on a variety of properties including the crystal structure of the grains, average grain size, water content, density and number of layers, making it challenging to definitively quantify global optical properties of snow [35]. Although very little research has been conducted on optical properties of snow in relation to PV, research from areas such as hydrology and geology can be used to understand it's properties. With regards to PV, two main optical properties of snow are of interest: reflectance (albedo) and transmittance. It has been accepted by many [36, 37, 38], that packed snow 2–3 cm deep have reflectance values from 70–90 % and will reach a maximum around 4 cm [36].

It has also been found that a thin layer of snow will have a dramatic impact on radiation transmission. Perovich [37] found that a snow thickness of 2 cm will reduce the transmission by 90 % and a 10 cm thick layer of snow can reduce visible light by 95 % and IR transmission by 99 %. Conflicting results from Järvinen and Leppäranta [39] claim that a snow depth of 47–74 cm is needed to reduce transmission by 99 %. Although the aim of this thesis is not specifically to look at the optical properties of snow, these values will help with analysis in subsequent chapters.

3.1.3 Module Cleaning and Snow Removal

Certain effects such as higher efficiency of PV in colder temperatures and increased reflectance from snow make cold climate regions a preferred location for PV systems. Therefore, snow removal solutions have been of great interest in recent literature. A report by Jelle et al. [40] summarizes the current challenges with snow removal and possible solutions. They suggests that the most logical solution is to chemically enhance the surface of the modules to prevent snow from accumulating or enabling snow to easily slide off.

Another solution that has been extensively researched is to heat up the modules to melt and remove snow. However, as Jelle et al. [40] point out and as mentioned in Chapter 1, a main driver for the increase in recent PV installations in Norway is policy, specifically the new EU policies around net-zero buildings [5]. Snow removal by energy consumption is therefore not the most optimal solution. Furthermore, a recent study by Frimannslund [41] concluded that the logistical problems of transporting melted snow away from the modules are problematic.

3.1.4 Effect of Snow on PV Performance

The overall effect of snow on PV energy production is evidently dependant on many factors including the module tilt angle, the thickness of snow layers and consequent optical properties, and how quickly the snow melts. After observing a test site in Ontario, Canada for two years, Andrews et al. [32] found that yearly losses due to snow ranged from 1 –3.5 %. It should be mentioned that low levels of snowfall were experienced during the test period compared to historical data, which may have decreased the overall losses over the two year period. Although trends were weak, it was observed that a lower temperature and higher relative humidity will increase the time it takes for snow to shed. As Trondheim has experienced a recorded average temperature of 0 ° with an average humidity of 76 % [42] over the past 10 years, the time for snow to slide off would be relatively shorter, therefore decreasing the overall effect that snow has on energy production [32].

Andrews et al. [32] also observed that the dependence of snow shedding on module angle was less pronounced, most likely due to the fact that the main shedding mechanism was melting rather than sliding. A study by Northern Alberta Institute of Technology [43] found that modules with a tilt of 14 ° experienced a loss in energy production of 16.78 % compared to 0.53 % at a 90 ° tilt angle. The results show a clear linear relationship between tilt angle and losses due to snow.

Lastly, a preliminary, unpublished study at NTNU by Gina Opstad Andersen [44] found that a 1 cm semi-uniform layer of snow resulted in a 50 % reduction in the MPP of a module at STC.

3.2 Effect of Partial Shading

To fully understand the impact that snow has on PV power production, the effects of shading and partial shading must be evaluated. The obstruction of light due to shading, soiling and weak lighting conditions has been studied extensively and is a key factor in understanding PV energy production in Norwegian climates.

Partial shading is one of the main causes of reduced efficiency in PV modules [45]. It occurs due to a variety of external elements such as passing clouds, neighbouring buildings and other structures, nearby trees, and snow. In partial shading conditions, PV modules receive different values of solar irradiation. This creates current mismatching, causing the shaded cells to act as a resistor and consume energy generated by neighbouring cells. Furthermore, the I-V curve of the array will contain several local peaks instead of one clear maximum peak as

shown in Figure 3.1a [46]. Standard MPPT methods often have difficulty differentiating between the peaks and therefore may not pick out the true global peak, causing significant power losses (Figure 3.1b) [47].

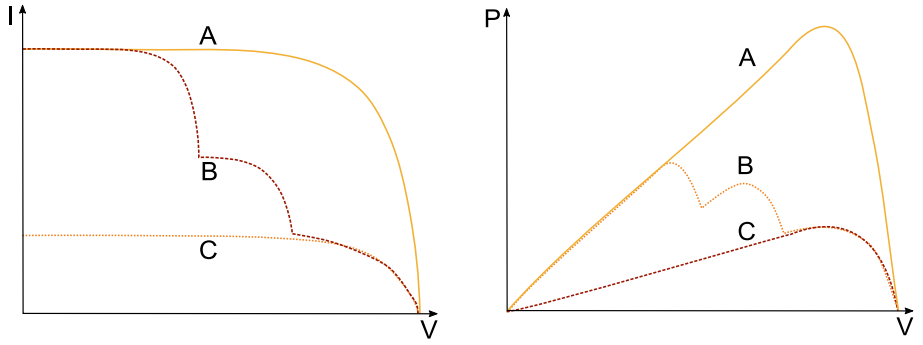

(a) (b)

Figure 3.1: I-V and PV characteristic curves of a PV array. **A** - uniform irradiation, **B** - partial shade with bypass diodes, **C** - partial shade without bypass diodes. Adapted from [48].

The impacts of shading vary depending on the type of modules, bypass diode placement and string configuration. When a group of cells experience shade and the bypass diode is activated, the voltage of the module will decrease by the sum of the voltages protected by the bypass diode plus the diodes forward voltage. The relationship between the effect of shade and power output is not linear, meaning that a small portion of shade may cause a large reduction in power output in the module.

A study on partial shading by Alsayid et al. [49] based on SimuLink simulations, found that a module consisting of two series connected groups of 18 series connected cells and two bypass diodes under STC produced at a maximum power of 140 W, as expected. When the same module was simulated under 50 % shading for half of the cells, a maximum power occured at 80 W. The same comparison was performed experimentally and obtained a value of 110.48 W for an unshaded module compared to 49.15 W when half of the module experienced significantly less irradiation. From this simplified shading example, it can be concluded that partial shading of modules can reduce the power output by around 50 % [49].

Additionally, Dolara et al. [50] found that shading 50 % of a single cell can reduce the power production of a module by more than 30 %. It was also observed that the effects of partial shading are very similar for both multicrystalline and monocrystalline cells. Furthermore, the power generation of

the cell is not dependant on the orientation of shading (horizontally, vertically or diagonally), however the power output of the entire module is of course greatly affected by the orientation of shading. For example, horizontal shading will influence all strings in the module due to the standard orientation and therefore has a greater impact [50].

3.2.1 Approaches to Avoiding Shading Losses

In reality, losses due to partial shading are not something that can be entirely avoided. To mitigate these losses, technical approaches have been explored. These solutions include the following:

- PV array configurations
- PV module configurations
- Module Level Power Electronics (MLPEs)

Array Configurations

A recent study by Bingöl and Özkaya [45] modelled five different array configurations and compared them under different shading conditions. According to experimental simulations, a total-cross-tied (TCT) configuration where all cells are all connected in a grid like pattern performs best. For a randomized shading pattern the TCT configuration provided a MPP of 1002 W compared with 730 W for a series configuration. Under uniform conditions, the MPP was 1722 W for all configurations.

A study by Belhachat and Larbes [46] showed similar results. It can be concluded that a TCT array configuration is preferable if shading can not be avoided. However, a significant loss is still experienced compared to uniform conditions.

PV Module Configurations

Module configuration have been researched by Lu et al. [51] to find an optimal module to mitigate partial shading losses. Three modules were compared; a standard 72-cell module with 3 bypass diodes, a series of 6 matricies, each consisting of two parallel strings of 12 halved cells, and a third configuration where two half cells are connected in parallel, and all connected in series with 3 bypass diodes.

According to the simulation results, the latter two performed best under partial shading conditions. Simulations ranging from 0–1 % shading resulted in differences

in power losses between the modules ranging from 1–20 % where the difference in losses appear to be greatest from 0.3–0.8 % shading coverage.

MLPEs

MLPEs, such as DC power optimizers and microinverters, are one of the fastest growing industries in PV systems. Whereas standard string inverters collect the data from the entire string and optimize the total power, DC power optimizers are attached directly to each PV module to optimize the power before the DC voltage is sent to the inverter. A microinverter performs the same task as a string inverter, converting DC into AC, but the conversion is performed directly at each module instead.

The advantage of both DC optimizers and microinverters is that the MPP of each module is the unaffected by the rest of the system. This has great advantages when PV systems experience partial shading. The main factor when deciding between MLPEs and a standard MPPT and string inverter is the cost [52]. In Chapter 6, an economic analysis will be formed on a small test site to compare the cost-benefit analysis of using microinverters in a PV system under partial shading.

Chapter 4

PV System Design and Evaluation

The following chapter outlines methods used to model the test site, located in Børsa, as well as the methods and equipment used to monitor the system. An explanation of the methods used during the economic case study on partial shading is also provided.

4.1 Solar PV Design and Simulation Software

The worldwide growth in demand for commercial and residential PV systems has resulted in the development of many PV design and simulation software packages. These software packages are a useful tool used by PV engineers, researchers, and architects to perform technical and economical plans and assessments of potential PV installations. All software packages are relatively user friendly, therefore ease of use was not included in the criteria.

Depending on where the software was developed, some packages cover a limited geographical range. For example, System Advisor Model (SAM) [53] and Homer Pro [54] are two software packages developed by NREL, largely used in the United states, which are only available for use in the United States, North and South America and Southern Asia [55]. An obvious requirement for this thesis is that the software package must include Norway in it's data library. The PV software packages considered for this project were:

PV*Sol Developed by Valentin Software (Germany) [56]

PVSyst Developed by PVsyst SA (Switzerland) [57]

PVGIS Simple and free software developed by JRC (Joint Research Center) from the European Commission [58]

PolySun Developed by Vela Solaris (Switzerland) [59]

Although recent studies have been published comparing the accuracy of various software packages, ultimately the accuracy is heavily dependant on the accuracy of input data and therefore varies greatly between different geographical areas and what data is made available [60]. A study has been made focusing on the

capabilities of each package based on the requirements for this specific project. These requirements include:

Climate database	Does the database contain a wide range of climate data that can be used in the model.
User input data	Is the user able to input custom data into the system to gain more accurate results.
Range of system components	Does the software have a wide range and newly updated package of modules, inverters and other electrical components.
Range of system configurations	Does the software have a wide range of possible configurations including grid connected and off grid systems.
Shadow analysis	Is the software able to include 3D shading elements and horizon profiles into the simulations.
Environmental analysis	Can the software calculate emissions savings based on current energy mixes.
Economic analysis	Does the software consider feed-in tariffs and other incentives to calculate energy savings, payback period and other financial indicators.

Table 4.3 summarizes the capabilities of each software package based on the requirements outlined above. Based on the outcome, PV*Sol software was used for all the design and simulation aspects of this project, due to the capability to model in 3D and add in nearby 3D shading elements.

Table 4.3: Summary of PV Software.

	PV*Sol	**PVSyst**	**PVGIS**	**PolySun**
Robust climate database				
User input data				
Wide range of system components				
Wide range of system configurations				
Shadow analysis				
Environmental assessment				
Economic analysis				

● Good ● Fair ● Poor/non-existent

4.1.1 PV*Sol Design and Simulations

PV*Sol was developed by Valentin Software and is currently one of the leading PV simulation tools in Europe. As indicated in the previous section, the PV premium package allows users to model both grid connected and off grid residential, commercial and power plant scale systems up to 100 MW_p. The site can be built in 3D, evaluated using 2D shade analysis and includes a large database of more than 5 000 commercial modules and 1 200 inverters. It has comprehensive climate data from 8 000 global locations. All components and climate data can be modified if necessary and it offers a lot of flexibility in the design and configuration of arrays. Aside from modelling the production, feed-in tariffs and incentives can also be implemented in order to calculate a financial overview [61]. The main purpose of the PV*Sol simulation in this thesis is to provide a benchmark in which to compare the recorded energy production of the system.

The test site was designed in PV*Sol using information provided by the owner of the installation. A more detailed description of the design constraints can be found in Appendix B. The following method was used to design the system:

1. Typically, the location of the site is entered into the program and the nearest weather station from the meteonorm database is then determined, in this case, Værnes. However, PV*Sol allows for the user to upload measured or more current weather values into the model in the form of hourly ambient temperature, wind speed, humidity, and irradiance. To

achieve the highest level of accuracy, the yearly values were taken from a nearby weather station in using measurements from Jan. – June 2018 and June – Dec. 2017 [62]. Monthly ground reflection (albedo) data was entered into the simulation parameters (Table C.2). The data was taken from the NASA Atmospheric Science Data Center and was averaged over 20 years from 1983 to 2005 [63]. Table C.3 shows the initial inputs taken from PV*Sol.

2. The residential building was designed in 3D in PV*Sol based on technical drawings provided. The final 3D model is shown in Figure 4.1.

3. The modules were configured onto the roof of the building in PV*Sol. Since SunStyle Sunroof is a relatively new type of module, it was not available in the technical database and was therefore entered manually using the technical data sheet. The modules were configured with 3 inverters and configured to match as closely to the original technical drawings as possible (Figure B.1). Table C.1 shows the technical inputs that were entered into PV*Sol.

4. Since Børsa is located in a valley, a horizon profile was implemented in order to account for topographical formations as shown in Figure C.1. The horizon profile data was taken from PVGIS tools [64]. It should be noted that the profile only takes into account long distance non-transparent shading elements (mainly landscape features such as mountains) and does not include nearby structures such as trees or neighbouring houses.

5. Once all of the system components are entered into the system, the simulation is run to determine the shade frequency of each panel (Figure B.4). This is an important tool that can help designers and planners determine the optimal placement of PV modules.

6. A yearly simulation is then run based on all inputs entered into the system and the production forecast is calculated.

4.1.2 Simulation Results

Based on the input parameters outlined in this chapter, the PV*Sol simulation calculates the yearly energy production of the system. The system is forecasted to produce 5 530 kWh/year. As seen in Figure 4.2, there is a large variance between winter and summer months. This is to be expected since Norway, and more specifically Trondheim, experiences long summer days and short winter days

Table 4.4: Overview of the BIPV test site in Børsa, Norway

String	Modules	Quantity	Inverter Type	Size [kW_p]
1	Sunstyle SolarRoof	15	Steca 1500 string inverter	1.26
2	Sunstyle SolarRoof	25	Steca 2500 string inverter	2.52
3	Sunstyle SolarRoof	26	Steca 2500 string inverter	2.31

due to its geographical location. For example, the expected energy output in December is 1.27 kWh compared to 984 kWh in May.

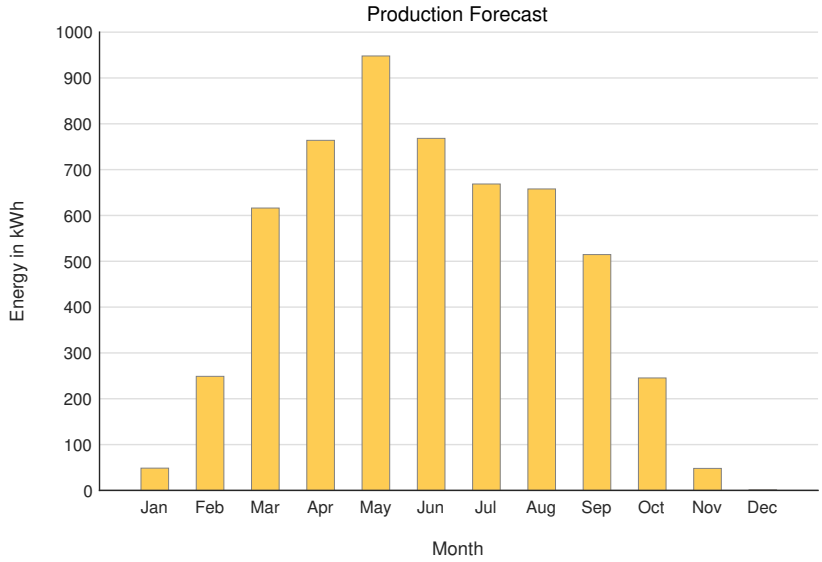

Figure 4.2: Monthly PV energy output from BIPV test site from PV*Sol simulation.

4.1.3 Measuring Snow Losses

A straight forward approach was taken when measuring the energy losses due to snow. According to a study by Marion et al. [65], the measured snow losses can be calculated by the following equation:

$$E_L = E_E - E_M \tag{4.1}$$

Where E_L is the energy loss due to snow, E_E is the estimated value of energy produced by the system and E_M is the measured energy production.

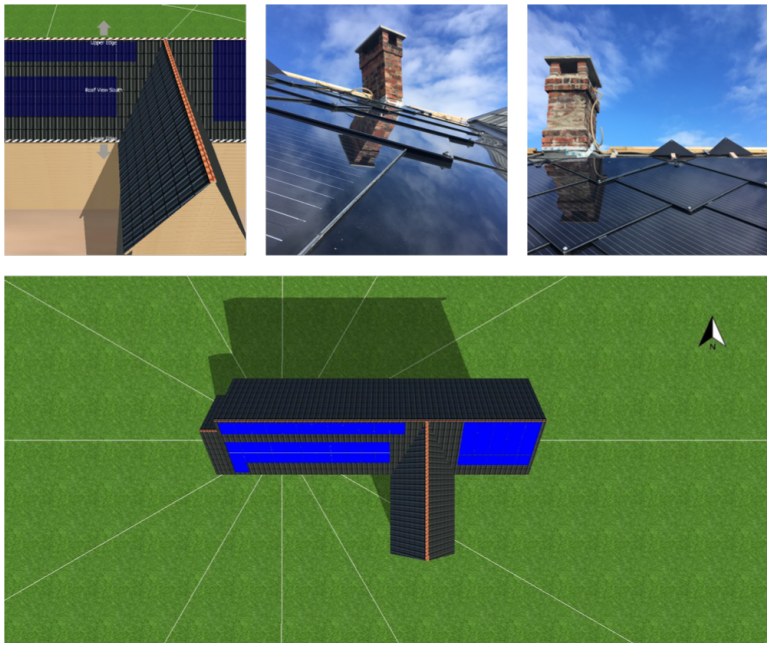

Figure 4.1: Model of BIPV system as designed in PV*Sol. The upper right and middle images show the actual roof to compare with the modelled system in the upper left and bottom image.

Another approach taken by Andrews et al. [32] was to calculated a modelled output ratio (M_{OR}) which is defined as:

$$M_{OR} = \frac{I_{sc}}{\widehat{I_{sc}}} \tag{4.2}$$

Where $\widehat{I_{sc}}$ is the modelled short circuit current and I_{sc} is the measured short circuit current. This approach was not viable due to an issue with data logging at the inverter, which prevented measured I-V characteristics from being recorded.

A combination of both approaches was used to calculate the loss of energy due to snow. A modelled output factor was calculated by taking the ratio of the measured energy output over the modelled energy output.

4.2 Measurement Tools

In addition to modelling the system in PV*Sol, various measurement tools were added to the test site in order to gain a better insight into the behaviour and energy output of the modules. Firstly, a data logger was programmed to record

the current systems performance at a frequency of 10 minutes. The data logged from the inverter and instrumentation included the following:

Temperature Sensors

Six temperature sensors were placed on the backsides of modules in order to gain insight into the temperatures of the modules, with little influence from T_a.

Pyranometers

A pyranometer works by responding to changes in temperature when sunlight heats a black surface. The pyranometer produces a voltage signal that is calibrated to be proportional to the direct irradiance. Since pyranometers accept light from all angles and producing a stable output regardless of the weather or sky conditions, they are most useful for comparing and predicting PV performance to historical data [66].

Two pyranometers were installed on the test site as shown in Figure 4.3. Pyranometer 1 is angled horizontally to record the solar irradiance in the horizontal plane. Since most weather stations measure irradiance on the horizontal plane, the data gathered from the test site could be potentially compared to other weather stations in Norway. Pyranometer 2 measures the irradiance experienced by the modules at 37°. The data from pyranometer makes it easier to directly compare the irradiance with the energy ouput of the system.

Reference Cells

A reference cell is similar to a pyranometer in that it measures irradiance, yet it works in a different way. The reference cell is made up of a PV material that should correspond to the system, in this case, mono-crystalline silicon. Similar to a PV cell, the reference cell generates a current dependant on the portion of the spectrum that is able to be absorbed. The voltage is then measured across a small resistor to measure the current. All reference cells are calibrated to STC. Since the reference cell only absorbs certain spectra based on the materials used, it is able to measure the irradiance that is available to the PV modules. Reference cells give a more exact characterization of the PV performance with quick time response [66].

The reference cell in this system was installed at the same angle as the modules (37°) to get an accurate reading on the solar irradiation that the modules experience, as shown in Figure 4.3.

Figure 4.3: Pyranometer 1, 2, and reference cell installed at test site.

IV Characteristics

As previosuly mentioned in Chapter 2, IV characteristics of PV are crucial to understanding what is happening at the module and system level. The AC and DC current, voltage and power as well as the AC frequency was logged on the test site. Having both AC and DC characteristics makes it possible to observe any losses that may occur across the inverter.

Measurement Challenges

It should be noted that this project faced some challenges in regards to measurement and data collection at the test site outside of Trondheim. The system was installed in mid-2017 by a Norwegian installer, and this aspect of the project was outside of the scope of this thesis. Although the issues were eventually resolved, the amount of data collection during winter months was greatly limited and disjointed. Specifically, the second string of the test site in Børsa was not properly recorded. Therefore, all results presented in this thesis regarding the test site in Børsa are based on results from the first string connected to Inverter 1.

4.2.1 Timelapse Imaging

In order to understand the affect that snow has on the output in a quantifiable manor, an attempt was made to calculate the area of the panels that were covered

by snow by recording still images at 10 minute intervals. Images were taken on a *Uovision UV785 Superb Full HD 12MP trail* camera, which was mounted on the west peak of the roof. These images were then processed using ImageJ [67] using the following steps:

1. Two consecutive images are opened and converted to 32-bit floating point (B&W).

2. Under the *Process* tab, *Image Calculator* was chosen.

3. The images are then subtracted from each other such that $img1 = img1 - img2$. In this case, the older image was subtracted from the newer image such that $img2 = img2 - img1$.

4. The resulting image was then subjected to thresholding under *Image–>Adjust–>Threshold*. Since each day presented different lighting conditions, the thresholding limits were carefully decided manually by comparing the processed image with the original.

5. Regions of Interest (ROIs) were drawn for each module and individual measurements were run to calculate the percentage of area covered.

6. This data was then used to quantify what percentage of each panel was covered by snow based on a time-series analysis. Data from the power output of the system was then compared directly to the amount of snow and ice coverage.

Image processing is cumbersome to run manually, therefore, a macro was recorded and run to automate the process. Due to difficult lighting, some images were manually adjusted. When a layer of snow was present on the modules, the measurements were more accurate due to the stark contrast between the white snow and the dark modules. However, times when there was either large amounts of reflection in the camera, ice formation on the modules, or during the start and finish of a snowfall, the data needed to be assessed manually by comparing the original image to the processed image and adjusting the threshold limits image by image. An example of the original vs. processed image can be found in Appendix A (Figures A.1, A.2, A.3, A.4).

Much attention has been paid to image processing of larger solar parks using techniques such as aerial thermography to detect defects and failures in large array [68]. More recently, interest in detecting soiling due to snow and sand has been

present in literature [69, 70]. This method of image processing was chosen due to its simplicity and the ability to manually manipulate measurements to gain more accurate results. Had the data set been larger, a more robust image analysis process would have been necessary.

4.3 Affects of Partial Shading

To fully understand how partial shading of snow affects the energy production of a system, a technical and economic analysis was performed on a commercial rooftop system in Oslo. Firstly, different shading scenarios were measured in a lab setting on a standard module. These shading scenarios were then carried out on the test site in Oslo. An technical and economic analysis was then carried out to understand the optimal system configuration.

4.3.1 I-V Curve Measurements

I-V curves were measured by Nicholas Riedel in DTU Fotonik's Class AAA Ecoprogetti solar simular. The module used was a 60 cell c-Si Gaia solar module with three bypass diodes. Each bypass diode contains 20 cells in series. This module was chosen as a representative of typical mono-Si modules. Figures 4.4, 4.5, and 4.6 show the comparison between the eight different shading orientations that were measured.

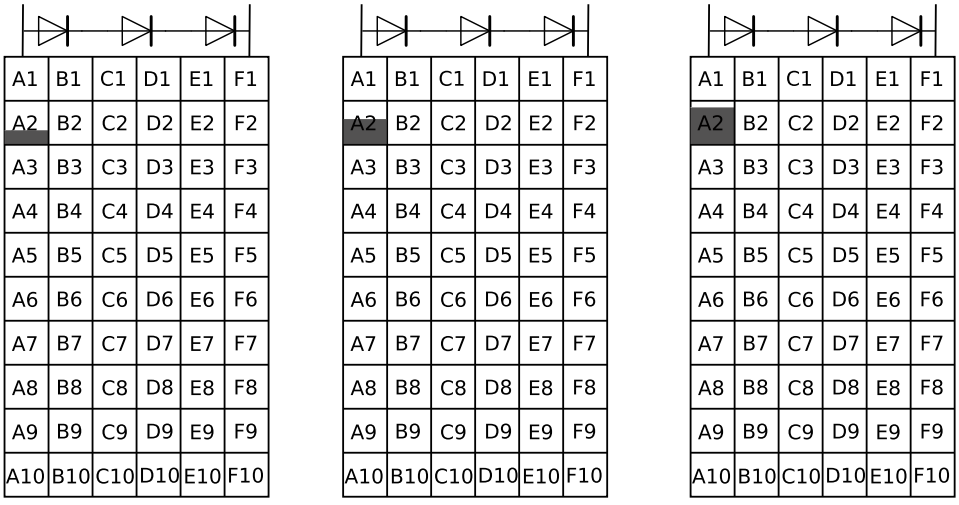

(a) A single cell, A2, is covered by 30 %.

(b) A single cell, A2, is covered by 57 %.

(c) A single cell, A2, is covered by 79 %.

Figure 4.4: A schematic representing a 60-cell module with 3 bypass diodes, where a single cell is covered by varying amounts.

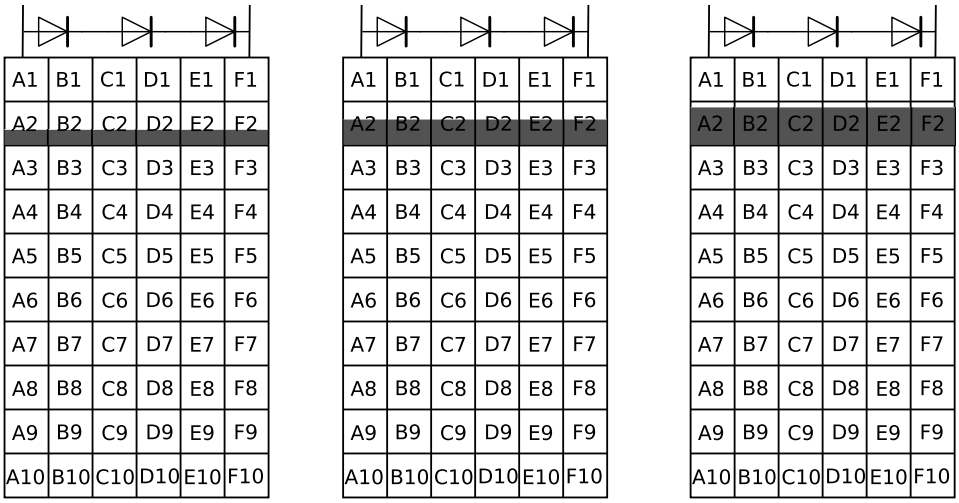

(a) The entire Row 2 is covered by 30 %.

(b) The entire Row 2 is covered by 58 %.

(c) The entire Row 2 is covered by 78 %.

Figure 4.5: A schematic representing a 60-cell module with 3 bypass diodes, where the entire Row 2 is covered by varying amounts. Row 2 extends across all three bypass diodes.

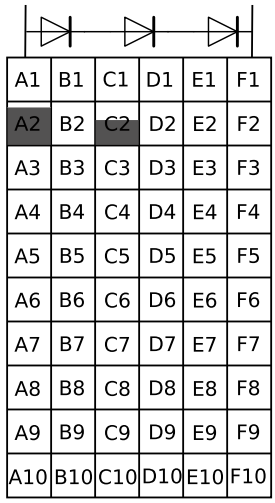

(a) A module where cell A2 is covered 79 % and C2 is covered 58 %. Both cells are connected to different bypass diodes, whereas the third bypass diode has no shaded cells.

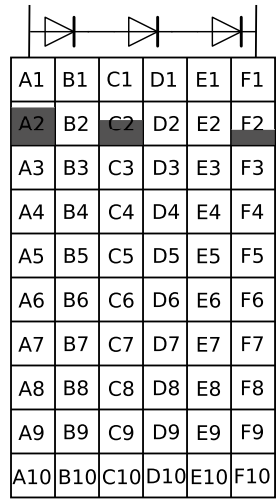

(b) A module where cell A2 is covered 79 %, C2 is covered 58 %, and cell F2 is covered 30 %. All cells are connected to different bypass diodes.

Figure 4.6: A schematic representing a 60-cell module with three bypass diodes, where the multiple single cells are covered by varying amounts.

Chapter 5

Affect of Snow on Energy PV Production

This chapter presents the results obtained from the methods described in Chapter 4. Mainly, the effect of snow and partial shading on PV energy output are presented.

5.1 Analysis of Snow

The effect that snow has on a PV system is of great interest in Northern regions, and varies depending on the specific climate of a region. Effects of snow were observed on a rooftop BIPV system in Børsa, Norway.

5.1.1 Overall Effect of Snow on Energy Production

To analyze the effect of snow on the energy output of the test site, an output ratio was calculated as described in Chapter 4. However, since the general accuracy of PV*Sol in Norway is unknown, a comparison of similar sample size was first calculated without the presence of snow. The results of both comparisons are presented in Figures 5.1 and 5.2.

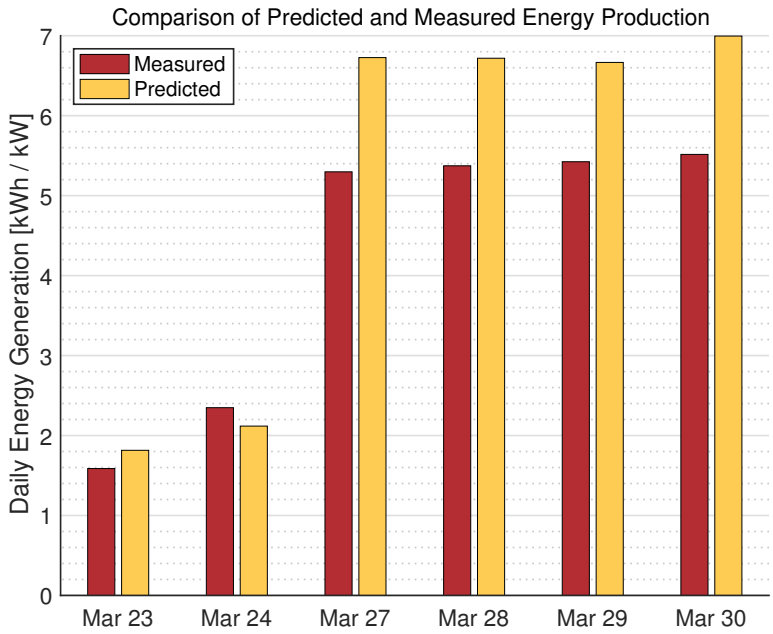

Figure 5.1: A comparison of predicted and measured daily energy output without the presence of snow.

The days when no snow was present showed an average energy output ratio of 0.86 $\pm$ 0.11. Since the model contains measured hourly values of irradiance, ambient temperature, wind speed, and humidity, the main source of error must come from other sources of inaccuracy. As mentioned in Chapter 4, albedo from snow can vary depending on the type of snow. A monthly average was entered into the model, which may account for some error. Furthermore, the model does not account for clouds or sky clarity, which means that typically cloudy winter months in Norway could also have contributed to some inaccuracy.

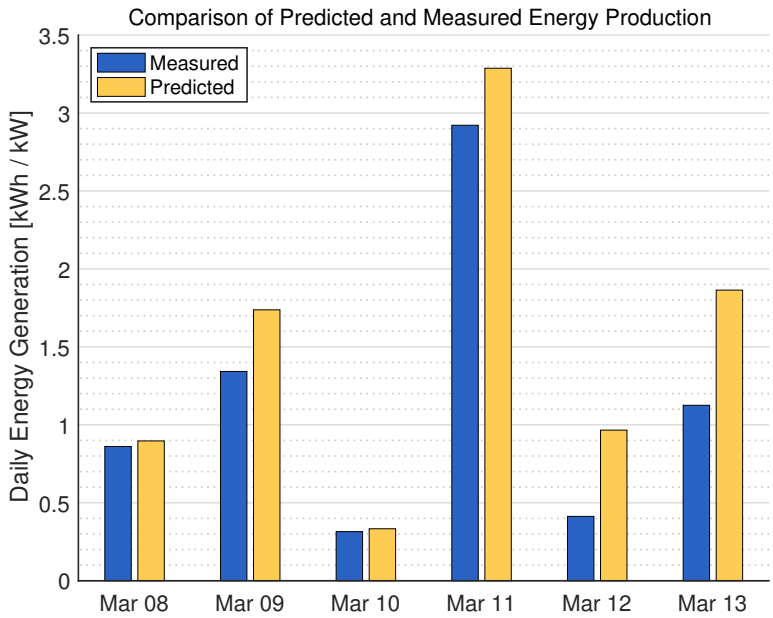

Figure 5.2: A comparison of predicted and measured daily energy output when snow was present at some point during the day.

The days when snow was present resulted in an average energy output ratio of 0.77 ± 0.19. The larger standard deviation may be due to the paradoxical effect of snow: When covering PV modules, it can greatly decrease the energy output, but when it is surrounding the modules, it can provide an increase in the diffuse solar irradiation.

5.1.2 Interpretation of Snow Coverage

The original aim of performing image analysis on the test site was to quantify the snow coverage and correlate that to energy production. However, the chosen method posed some challenges. Firstly, the snow coverage is time dependant, making it difficult to definitively correlate a snow coverage value to an energy output ratio. As discussed in Chapter 3, the properties of snow vary greatly, and through image analysis it is difficult to determine the type of snow as well as the thickness of the layer. Furthermore, the mountainous landscape of Norway makes it very difficult to obtain accurate snowfall data, as each weather station varies in altitude. However, some qualitative observations can be made.

Figure 5.3 shows the calculated hourly snow coverage compared to the daily energy output ratio, where each day represents the hours from sunrise to sunset. It can be seen that the energy output ratio is the lowest during March 12 when

snow covers the panels during the middle of the day. This is expected as the solar irradiation is highest during the middle of the day and when the angle of the sun from Zenith is highest. The highest energy output ratio occurs on March 8. This is not surprising as the modules are covered in the morning and the snow quickly melts.

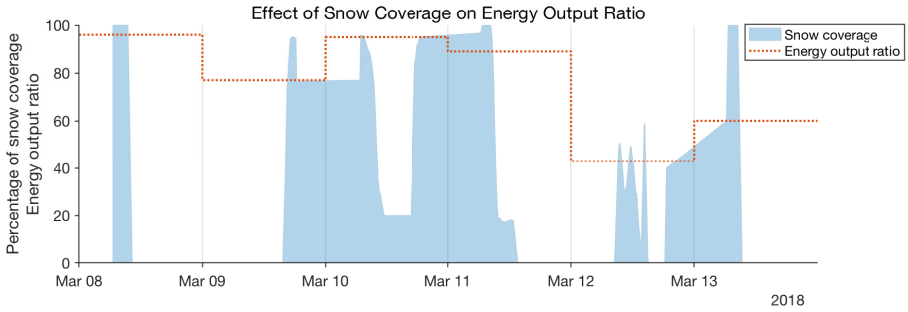

Figure 5.3: Calculated hourly snow coverage compared to the daily energy output ratio.

It is interesting to note that the energy output ratio is also quite high on March 10., even though at least some of the modules are covered over the entire day. It would be expected that the partial shading of the string would greatly reduce the energy output.

5.2 Analysis of Partial Shading

The effects of snow on energy output are not only present when the PV system is entirely covered. When only parts of a module are covered by snow, partial shading comes into effect. To explore the effects of partial shading, a total of nine shading scenarios were simulated on a typical three diode PV module, as described in Chapter 4, and the I-V curves were measured. In addition to these nine laboratory simulations, similar shading scenarios were then carried out on a commercial rooftop PV system to study the effects on the overall energy output of the system. In this chapter, prominent results from the simulations are presented. An economical assessment on the rooftop system will follow in the subsequent chapter.

The nine shading simulations were designed to mimic possible outdoor shading configurations that were imposed onto the rooftop test site. A summary of results can be found in Table D.1.

Single Cell Shading Simulation

The first set of simulations presented show a shading scenario where a single cell on the first column of the module was covered by a varying degree. It can be seen from Figure 5.4 that as the shaded area of the cell increases, the MPP of the module decreases exponentially and therefore the FF decreases.

All scenarios have similar V_{oc} and I_{sc} values in relation to the unshaded module. This is to be expected since a drop in I_{sc} only occurs when there are no bypass diodes present. The current at the MPP is the lowest when the cell is shaded only 30 %. This is most likely due to the fact that the resistance created by the 30 % shaded cell is not large enough to redirect the current through the bypass diode. Once the cell is covered 57 % or more, the bypass diode is activated. This means that Columns C–F will operate at a higher current, but with a more significant voltage drop due to the voltage loss from Columns A and B. These results are consistent with the literature presented in Chapter 3 which found that a single cell shaded by 50 % would result in a loss of 30 %.

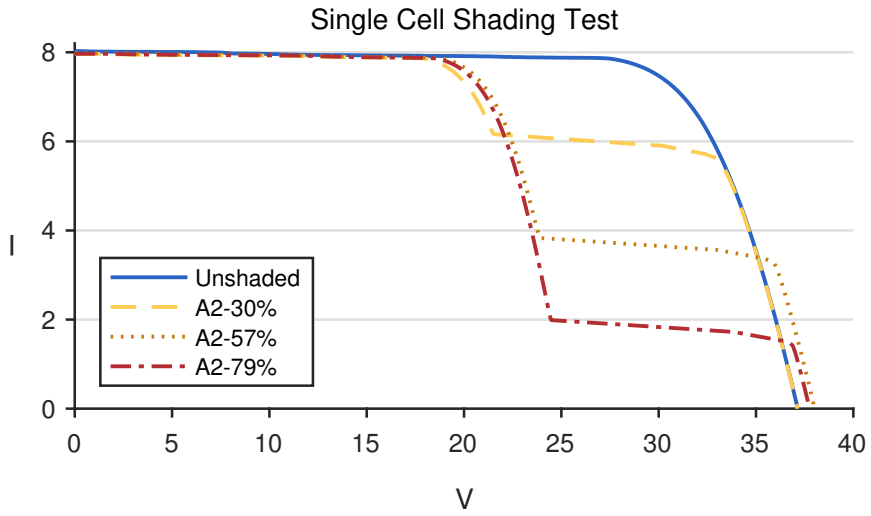

Figure 5.4: Resulting module I-V curves when a single cell is shaded in varying amounts compared to a fully unshaded module.

Multiple Cell Shading Simulation

The next set of simulations presented in Figure 5.5 show the affect of having multiple cells shaded in parallel in varying amounts. Both scenarios show a loss in the MPP of 65 %. In the first case, two shaded cells in Column A and C belong

to two different diode strings, and Columns E and F are free to produce normally.

When three cells are shaded in Columns A, C and F, all bypass diodes are affected. There is no feasible way to avoid the shaded cells, causing the module to act as if no bypass diodes were present. This is indicated by a drop in the I_{sc}. The MPP is however higher for the module with three shaded cells compared to only two shaded cells. This can be explained by the fact that the module is more balanced, therefore decreasing the resistance which in turn produces a slightly larger current.

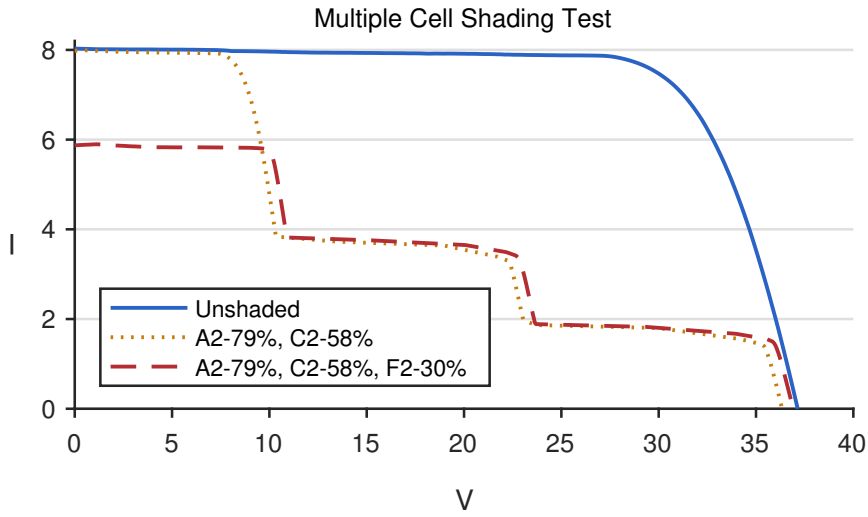

Figure 5.5: Resulting module I-V curves when a multiple cells are shaded in varying amounts compared to a fully unshaded module.

Single Row Shading Simulation

The final simulation set compares I-V curves when increasing amounts of area in Row 2 experience shading as shown in Figure 5.6. This means that uniform shading occurs across all three bypass diodes and therefore greatly affects the I_{sc}, or the maximum current that the module will experience.

The trend clearly indicates that an increase in the shaded area results in a decrease in the MPP, mainly due to a decrease in current. Furthermore, the simulation in which Row 2 was shaded by 78 % resulted in the lowest MPP of all simulations. This is due to the fact that the current produced in the unshaded area of Row 2 (12 %) determines the current of each cell in the entire module, since there is no way to bypass the entire row. This greatly hinders the power production of the module by 75 %. Literature presented in Chapter 3 showed similar results, stating "that losses between 20–90 % are possible with shading

that affects as little as one row of cells within a module." [71].

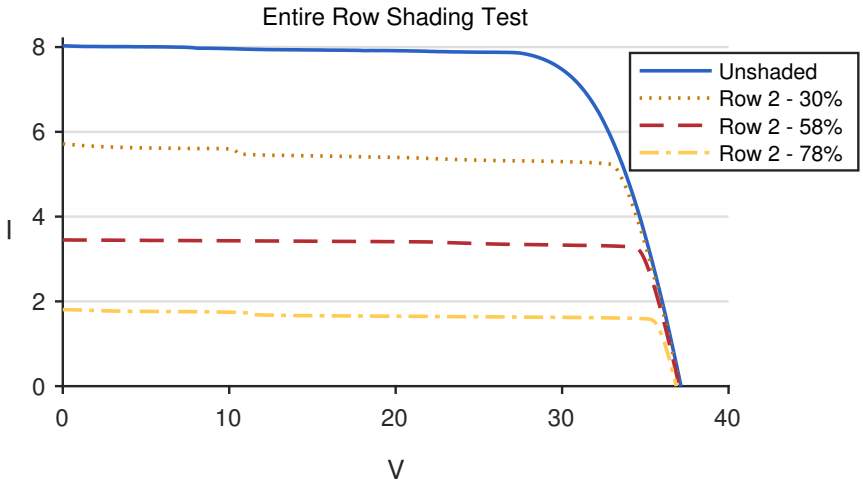

Figure 5.6: Resulting module I-V curves when an entire row of cells are shaded in varying amounts compared to a fully unshaded module.

Overall, this shading simulation reflects similar values to what is present in literature, and provides a strong basis to compare the subsequent results.

Chapter 6

The Economics of Shading

While understanding the technical limitations of a PV systems under various shading conditions is important, a main driver of the PV industry is cost. The objective of this chapter is to assess whether more advanced and expensive inverter technologies pay off when the energy output of a system is compromised by partial shading conditions.

The aim of this chapter is to compare the three inverter technologies from an economic standpoint. The test site is located in Skøyen on a south-west facing roof of a commercial building. Three inverter technologies were observed under three scenarios in which various amounts of shading were imposed on the system. The analysis took place in May 2018 during a period of sunny, clear days which means that shading from clouds had little influence on the results. The data was then used to make an economics assessment of the most cost effective inverter technology under the different shading conditions.

6.1 Shading Test-site Design

The test site was installed on the roof of Multiconsult's main office building in Skøyen in mid-2016 to be used as a demo system. The roof is south-west facing and has a total of 42 modules with a total dimension of 10.92 kW_p. The modules are tilted at 20 ° and facing S 40 °W. Figure 6.1 shows the layout of the system.

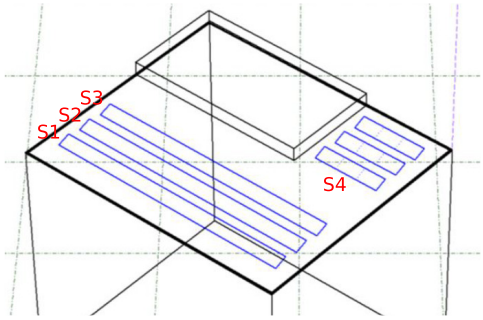

Figure 6.1: Layout of PV system on Multiconsult's roof.

The system consist of three strings with 11 modules and an additional smaller

string on the east side of the roof with nine modules. The first and third string are identical with the idea that the first string would act as a reference string while the third string would be subjected to shading. The modules in the second string are connected to DC optimizers and a string inverter that is best compatible with DC optimizers. Lastly, the fourth string consisting of 9 modules are connected to micro inverters. Each microinverter is connected to two modules which optimizes and inverts each module separately. An additional inverter is used due to the odd number of modules in the system. An overview of the system technology is presented in Table 6.1.

Table 6.1: Overview of the Multiconsult PV system design

String	Modules	Quantity	Inverter Type	Quantity	Size [kW_p]
S1	Polysol 260	11	StecaGrid string inverter	1	2.86
S2	Polysol 260	11	SolarEdge string inverter	1	2.86
			SolarEdge power optimiser	11	
S3	Polysol 260	11	StecaGrid string inverter	1	2.86
S4	Polysol 260	9	Micro inverter	5	2.34

6.2 Description of Shading Scenarios

To observe the effects of shading, three different scenarios were carried out during the month of May in 2018. The following list outlines the dates and a description of each shading test as shown in Figure 6.2.

Scenario 1 2018-05-03 - 2018-05-16 A strip of plastic 15 cm wide covering the full width of the module was placed on Strings 2–4.

Scenario 2 2018-05-17 - 2018-05-28 A strip of plastic 15 cm wide covering half the width of the module was placed on Strings 2–4.

Scenario 3 2018-05-29 - 2018-06-01 A pipe shaped shading element was placed in front of a module at Strings 2–4.

(a) Scenario 1: a 15 cm strip of plastic covering the entire width of the module.

(b) Scenario 2: a 15 cm strip of plastic covering half the width of the module.

(c) Scenario 3: a shading pipe casting a shadow on the module.

Figure 6.2: The placement of shading elements on PV modules at the test site on Multiconsult's roof in Skøyen. Photos taken by Anne Frederikke Østby at Multiconsult.

6.3 Analysis of Data Under Shading Conditions

During each shading scenario, the system experienced different weather conditions and therefore external factors such as temperature, irradiance and cloudiness will differ. The scenarios were also carried out under differing time frames due to time constraints. To account for these variances, each scenario has been normalized to the reference inverter, which remained unshaded through out the shading scenarios. A comparison between the performance of each inverter technology was calculated using a data set from May 2017 consisting of data points every five minutes. Additionally, the string connected to the micro inverters was dimensioned to represent the same size array as the other three strings to provide a more accurate comparison. These results are used as a baseline to compare the results under the three shading conditions as shown in Figure 6.3.

In theory, the standard deviation of a data set should decrease with an increase in sample size. However, each inverter technology could potentially behave differently through out the year based on large variances in energy output, temperature, irradiance and other external factors. Therefore, taking the baseline sample from May 2017 rather than the entire year resulted in a significantly smaller standard deviation. The month of May was chosen to be consistent with the month that the shading scenarios were carried out in the following year in 2018.

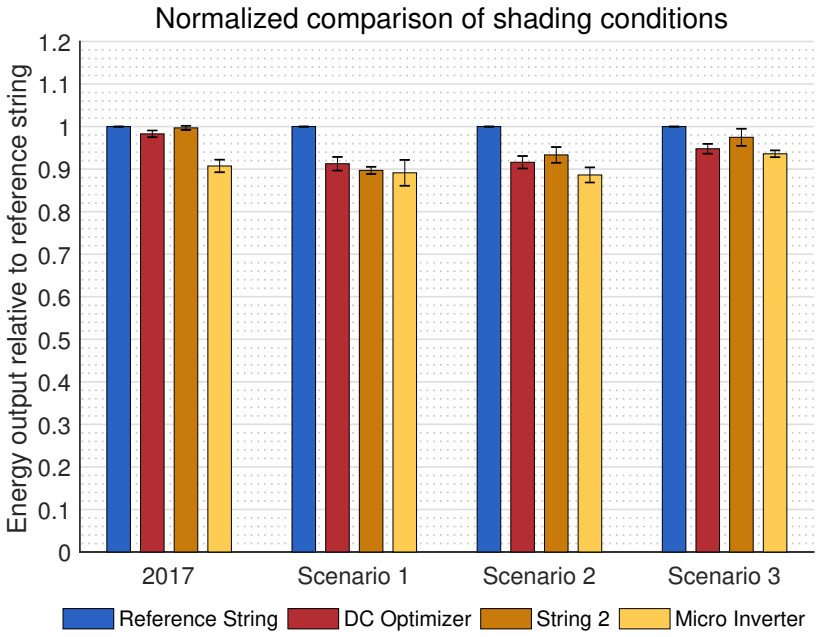

Figure 6.3: Energy output during May 2017 compared to the three shading trails carried out in May 2018, normalized to the reference string in each scenario.

Reference Scenario

The reference scenario taken from May 2017, has the smallest difference between each inverter technology. This is expected as each inverter should be performing at the optimal MPP without the influence of partial shading. Furthermore, both standard string inverters have the highest energy output. Since both DC optimizers and micro inverters allow each module to be optimized individually, it is expected that the energy output would be the highest between these two. One explanation could be that the DC optimizer and micro inverters have a lower efficiency, although this is highly unlikely.

Scenario 1

Scenario 1 shows that all three shaded strings are producing less than the reference string. This is expected due to losses from the shading on the other three strings. The DC optimizer shows the best performance compared to String 2 and the micro inverter. According to both the literature presented in Section 3.2 and the results from the partial shading study in Section 4.3, it is expected that the energy production from String 2 would be greatly decreased compared to the DC optimizer and micro inverter. However, this is not the case as String 2

experiences a loss of only 11 %.

As expected, the largest loss occurs in Scenario 1 when the entire width of the module is covered.

Scenario 2

According to the results from Scenario 2, when only half of the width of the module was covered, String 2 had the highest energy output. Again, this is unexpected since the modules are connected in series and therefore the reduced current in the shaded module will affect the entire string, greatly reducing the MPP.

Scenario 3

The third scenario, where a shading element was placed in front of a module in each string shows similar results to Scenario 2. String 2 has the lowest energy loss with a reduction of 2.5 %. It was expected that all strings would have a higher energy production since the shading element casts a smaller shadow than the area of plastic strips, and the length of the shadow changes through out the day. Furthermore, when the shading element casts a shadow, the panel still experiences some irradiance compared to when the light is completely blocked out as in Scenario's 1 and 2.

6.4 Economic Assessment

The economics of solar PV have been studied extensively worldwide to compare costs of emerging technologies, analyze trends, and predict changes in the market [72, 12]. As capital and operational costs associated with PV are rooted in the local economy, understanding the relationship between technical performance and cost is necessary to continue to grow a developed market. Recent studies from WWF Norway and Accenture [73] and The Solar Energy Cluster [74] present comprehensive findings on the current and future market of PV in Norway. However, a concrete comparison between technological and economical potential is lacking.

Cost Considerations

The costs associated with PV systems can be divided into four main categories: the cost of the PV modules, which can account for up to 50 % of the total system costs [73], inverters, balance of systems (BOS) which consists of all additional electrical components required, and lastly installation and labour costs [75, 73]. This assessment considers the capital costs associated with each inverter system along with a cost estimation of additional BOS components and installation.

Nina Jensen and Pål Ødegaard [73] report the standard average investment costs in 2016 for a residential PV inverter, additional BOS, and installation costs to be 2000 NOK/kW, 4400 NOK/kW, and 2500 NOK/kW respectively, representing 9.0 %, 20.8 %, and 19.5 % of the total investment costs. In this assessment, the costs of each inverter were between 3000 and 4500 NOK/kW as reported by the local installer in Norway. Typically, the cost per kW decreases as the size of the system increases which may account for the higher prices. It has also been assumed that all energy produced from the system will be used locally, meaning that all revenue streams used in the assessment will come from energy savings. Table D.2 outlines all assumptions and data used in the model.

Application of Costs

A levelized cost of energy (LCOE) is an economic tool used in the energy industry to compare the costs of various technologies per kWh of energy produced. While an LCOE is not the best tool to use when making investment decisions, for the case of this study, it provides a simple metric to compare each inverter technology based on the energy production in each scenario.

Figure 6.4 shows the comparison of the LCOE of the DC optimizers, string inverter and micro inverters under the three shading scenarios. While the micro inverter has a higher upfront cost, the ease of installation results in lower additional BOS and installation costs, resulting in a more valuable investment compared to standard string inverters [75, 12]. The DC optimizer has the highest total investment cost of 27 176 NOK/kW, however, the improved energy output under shading conditions compared to the string inverter makes it the more economical choice.

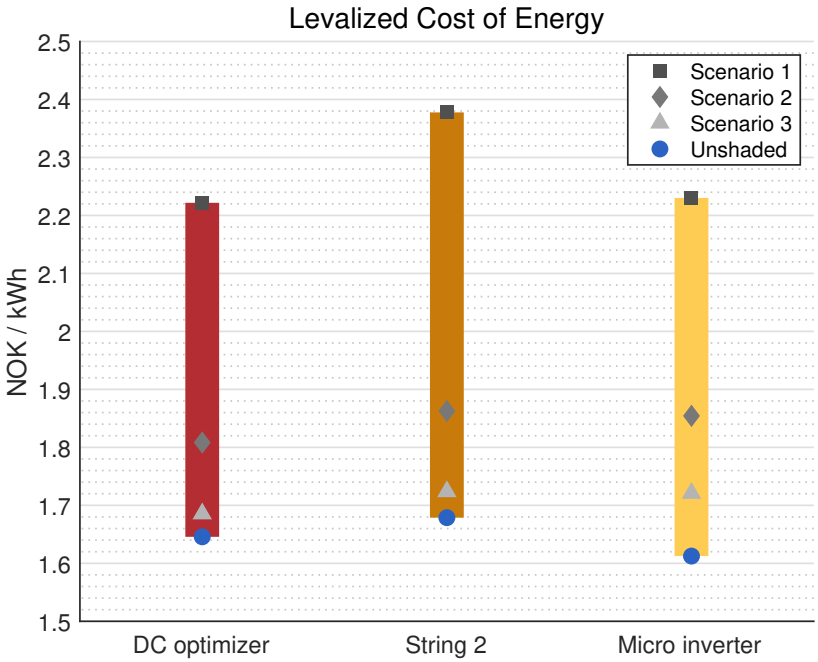

Figure 6.4: Results from the economic assessment showing the LCOE for a DC optimizer, string inverter, and micro inverter under various shading scenarios.

Chapter 7

Discussion

This chapter aims to reflect upon the results and analysis presented in the thesis in relation to the thesis objectives. This includes the comparison of the PV*Sol model to measured energy production, the effect of snow on PV energy production, and the effects of partial shading.

Based on the results presented in this thesis, some inferences can be made about the effect that snow and partial shading has on the performance of small scale PV systems. It should be kept in mind that the short duration of measured data in both test sites decreases the statistical significance of the results. Furthermore, larger variance in the results would be expected if the energy were to be measured through out the entire year.

7.1 Reflection on PV model

The model of the BIPV test site in Børsa was designed based on technical drawings that were provided, with the aim of being as precise as possible to obtain to most accurate results. When comparing the predicted energy output to measured energy output during days with no snow, the average energy output ratio was 0.86 $\pm$ 0.11. The reason for comparing such a small sample of daily values was due to inconsistency in the recording of measured values. To get a proper comparison of modelled and measured values, it is recommended that the system is monitored for a minimum of a year. Furthermore, the validity of the results rely on a variety of factors including weather, geographical and technical data. PV*Sol allows for the user to upload measured or more current weather values into the model in the form of hourly ambient temperature, wind speed, humidity, and irradiance. To achieve the highest level of accuracy, the yearly values were taken from a nearby weather station in using measurements from Jan. – June 2018 and June – Dec. 2017.

By using a horizon profile calculated from the geographical coordinates, the local landscape could be taken into account. To improve this data, a photographic shade measurement could have been implemented to build a more accurate 3D model of long distance shading elements surrounding the test site. In terms of shading losses, limitations in the design of the BIPV may have contributed to an increase in predicted energy output. As seen in Figure 4.1, the modules in the

model do not cover the entire roof and are not integrated into the roof as they are at the actual test site. This inconsistency may have decreases shading losses coming from other sections of the roof and therefore increased the predicted output.

Overall, the model predictions can be considered accurate enough to calculate snow losses in the month of March, but a further comparison using yearly measurements would greatly improve the validity of the model.

Models and predictions of PV energy systems are a vital tool used in the PV industry. The improvement of input data and prediction models to increase accuracy will lead to a more efficient use of PV technology, and therefore more cost effective solutions.

7.2 Characterization of Snow

According to the results from this thesis, losses due to snow resulted in an energy output ratio of 0.77 compared to an energy output ratio of 0.86 when snow is not present. This can be correlated to a loss of 11 %. However, the small data population due to issues with measurement recordings makes it difficult to determine the validity of these results. In order to calculate the overall effect that snow has on the yearly energy output of a system, a larger data population which extends over the entire period of winter would be preferred. Furthermore, this energy output ratio of 0.77 represents the losses only from days when snow was present. Therefore, the overall losses in the month of March would be less when days without snow are also included.

An interesting observation when analyzing the days when snow was present is the larger standard deviation between the daily energy output ratio. This is most likely due to the fact that when snow is present it is either covering the modules and hindering energy production, or it has been removed from the modules and surrounding snow leads to an increase in diffuse irradiation. Therefore, it is possible that the additional diffuse radiation from the albedo effect of snow may counteract the energy losses due to snow coverage.

Due to the issues with data recording, the temperature of the modules was not recorded during times of snow. To gain further insight into the effects of snow, it would be desirable to analyze how the snow affects the temperature of the modules, and therefore the overall efficiency of the system. Furthermore, the topic of tilt angle is widely discussed in the literature and is an important component in understanding the effects of snow on energy production.

7.3 Partial Shading Analysis

The results from the partial shading simulation show that an increase in shading decreases the MPP of the module, and as little as 30 % areal coverage of one cell can reduce the MPP by 18 %. Shading multiple cells further increases the reduction of power in the module. Shading across the entire width of the prevents the bypass diodes from being used, therefore having the largest effect on the MPP. Therefore, due to the design of standard PV modules as described in Chapter 2, the effects of shading on a module are dependent on the orientation of the shading.

The literature pertaining to partial shading of modules is extensive, and as expected, the results from the partial shading simulations presented in this thesis were consistent with the literature and the expected outcome. The findings from this work were presented to simply verify the effects of partial shading on the MPP of modules and have a benchmark to discuss further findings in this thesis.

The partial shading simulations were designed to emmulate the partial shading measurements at the roof-top test site in Skøyen. This is a valid comparison since the modules have a similar design with three bypass diodes, as well as a similar size and nominal output. Therefore, it is reasonable to expect that the modules at the test site will behave similarly to the shading simulation under the partial shading scenarios.

In the case of the BIPV test site in Trondheim, each module is equipped with only one bypass diode. While the basic principles of partial shading hold true, with only one bypass diode, it is expected that smaller areas could have a larger effect on the power loss of each module. For this reason, the specific orientation and area of partial shading due to snow coverage was not considered during the analysis. To further investigate the effects of partial shading due to snow on this system, similar partial shading simulations should be performed on the SunStyle Sunroof modules and compared to I-V characteristics measured on site.

7.4 Inverter Performance

Following the partial shading simulations, similar shading scenarios were measured on a test site in Skøyen. It was expected that the micro inverter string would perform best at all times since each module is independant of the other, therefore any soiling or shading impacts will not affect the rest of the string. Therefore, it is quite peculiar that the micro inverter string is consistently the worst performer.

Although the nominal output of the string is slightly smaller, it was re-dimenshioned to be comparable to be the same size as the rest of the strings.

One explanation may be the location of the system. As the micro inverter string is located to the east side of the building, the system may experience shading in the evening which was unaccounted for.

However, similar results were found for the string with DC optimizers. Similar to the micro inverters, the DC optimizers are also expected to improve performance as each module is optimized individually.

Perhaps the confusion does not lie within the results of the micro inverter or DC optimizer string themselves, but within the results of the shaded string inverter. In comparison, the standard string inverter should see a much larger loss in energy output under all three shading scenarios. According to results from the shading simulations, I_{mpp} of the shaded module should be reduced by approximately half. We also know from the literature and theory that each module in the string would be operating at this reduced current, which would greatly reduce the power of the entire string. Therefore, the energy output of the string inverter under shading conditions can not be explained.

7.5 The Cost of Inverter Technologies

The economic analysis presented in this thesis provides an insight into realistic costs associated with different inverter technologies under shaded and non-shaded conditions. Due to a lack of information, assumptions were made when assessing the BOS and installation costs, which represent a large portion of the overall system costs. This lack of information is merely a reflection of the lack of choice in the Norwegian PV market. As micro inverters and DC optimizers have gained popularity in American markets over the last five years, these options are simply not offered in Norwegian markets.

According to the results from this economic study, micro inverters and DC optimizers are an economically feasible solution that should be further developed and offered in the Norwegian residential PV industry. The results show that not only does the microinverter have a lower LCOE under various shading scenarios, but also under normal unshaded conditions. Furthermore, DC optimizers are a valuable addition to a PV system that can be installed on pre-exisiting systems to improve energy output and therefore improve the payback time of the system.

In regards to the costs of the inverters themselves, some deviations from the literature should be mentioned. In this specific case study, the costs of the micro inverters used in the installation was much cheaper than expected in comparison to the string inverter. Typically, a micro inverter is around double the cost of a string inverter, whereas this case study the micro inverter was 40 % more expensive.

Therefore, a more in depth comparison including a range of investment costs for each inverter technology would provide a more robust and valid conclusion.

It should also be kept in mind that this economic analysis was based on of the results from the shading scenarios presented in Chapter 6. Therefore, if the string inverter behaved as expected with a larger reduction in energy output, the LCOE would be even higher for the three shading scenarios.

Chapter 8

Conclusions

This chapter summarizes the findings presented from the work done over the course of this Master's thesis. The following conclusions can be made:

The Effect of Snow on Energy Production:

- The snow coverage on a residential BIPV roof PV system in Børsa, Norway was calculated by performing image analysis on timelapse images taken of the system. This method has proven to be a useful technique in quantifying the amount of snow covering the system.
- This project has shown that an average daily reduction in energy output of 11% can be measured when snow and ice is present on a PV system in Nordic climates.
- The overall effect of snow on a system may be mitigated by the increased diffuse irradiation when snow is present around the PV system but not covering the modules.

Partial Shading of Modules and Systems:

- Shading simulations were carried out on a typical mono-Si module with three bypass diodes to verify the effects of partial shading on energy output.
- The largest reduction in energy output occurs when a horizontal row of three cells are covered so that 78 % of its area is shaded. This results in a 75 % reduction in the MPP compared to an unshaded cell.
- To understand partial shading at a system level, three shading scenarios were analyzed and compared based on their relative output. The scenarios were carried out on a small scale roof top building in Skøyen, Norway.
- The results show that the lowest relative energy output occurred when a 15 cm strip was covered across half the width of the module at micro inverter string. However, the performance of the string inverter under all shading scenarios does not align with the relevant theory and literature. Therefore, a final conclusion can not be made.

Levelized Costs of Inverter Technologies:

- Energy output values from the shading scenarios in Skøyen were implemented into an economic analysis to compare LCOE for each inverter technology.
- The cost of the inverters, additional BOS costs, and installation and maintenance costs were taken into consideration. Assuming a rate of 4 % inflation in electricity costs and a system lifetime of 25 years, the string with micro inverters presented the lowest levelized cost under no shading, followed by the string with DC optimizers.
- When a module in each string was covered by a 15 cm strip around the entire width of the module, the string with DC optimizers presented the lowest levelized cost, followed by the micro inverter string.

8.1 Future Work

Based on the conclusions presented from the work pertaining to this Master's thesis, the following topics are recommended as the most important topics of research in the field of PV energy production in Norwegian climates:

- Firstly, it is recommended that further research goes into the relationship between the tilt angle of modules and snow accumulation in Norway to explore the impact on energy production.
- Great interest has been expressed in solar tracking systems to improve the energy yield in Nordic regions. Further research could also explore how tracking systems can be used to reduce snow accumulation on modules.
- One of the major challenges in Norway is access to outdoor testing and measurement sites. It is therefore proposed that test sites designed for the purpose of observing the effects of snow on energy output are built around Norway to study the effects of tilt angles, snow accumulation and system configurations.
- Finally, an increase in reliable measurement instruments will greatly improve all aspects of PV energy in Norway. Specifically, properly calibrated pyranometers in all regions of Norway would be of great benefit to the research community.

Bibliography

[1] IPCC. Climate Change 2014 Synthesis Report Summary for Policymakers, 2014. URL https://www.ipcc.ch/pdf/assessment-report/ar5/syr/AR5_SYR_FINAL_SPM.pdf.

[2] Solveig Aamodt, Carlos Sallé Alonso, and Guri Bang. Energy Transition Outlook 2017: A global and regional forecast of the energy transition to 2050, September 2017.

[3] United Nations Commission on Sustainable Development. The Sustainable Development Goals Report, 2017. URL https://unstats.un.org/sdgs/.

[4] Ministry of Climate and Environment. Norway's climate target for 2030, March 2015. URL https://www.regjeringen.no/en/aktuelt/innsending-av-norges-klimamal-til-fn/id2403782/.

[5] Andreas Hermelink, Sven Schimschar, and Thomas Boermans. Towards nearly zero energy buildings: Definition of common principles under the EPBD. Technical report, February 2013. URL https://ec.europa.eu/energy/sites/ener/files/documents/nzeb_full_report.pdf.

[6] International Energy Agency. Energy Policies of IEA Countries - Norway 2017 Review. URL https://www.iea.org/publications/freepublications/publication/energy-policies-of-iea-countries---norway-2017-review.html.

[7] Dr. Dorte Fouquet. Implications for the export of Norwegian renewable energy to the EU, February 2017.

[8] Tennet. International Connections, 2018. URL https://www.tennet.eu/our-grid/international-connections/nordlink/.

[9] North Sea Link - Projects, 2013. URL http://www.statnett.no/en/Projects/Cable-to-the-UK/.

[10] Nordic Investment Bank. Solar silicon production takes off in Norway. URL https://www.nib.int/news_publications/cases_and_feature_stories/167/solar_silicon_production_takes_off_in_norway.

[11] Øystein Holm. Trends in the Norwegian solar PV market in 2016 – comments. Technical report, IEA PVPS, 2016. URL https://multiconsult.no/assets/Kommentarer-til-Markedsutviklingen-2016_ENG.pdf.

[12] Ran Fu, David J. Feldman, Robert M. Margolis, Michael A. Woodhouse, and Kristen B. Ardani. US solar photovoltaic system cost benchmark: Q1 2017. Technical report, National Renewable Energy Laboratory (NREL), Golden, CO (United States), 2017.

[13] Fraunhofer Institute for Solar Energy Systems, ISE and PSE AG. Photovolatics Report. Technical report, Freiburg, July 2017. URL https://www.ise.fraunhofer.de/content/dam/ise/de/documents/publications/studies/Photovoltaics-Report.pdf.

[14] Martin A. Green, Yoshihiro Hishikawa, Wilhelm Warta, Ewan D. Dunlop, Dean H. Levi, Jochen Hohl-Ebinger, and Anita W.H. Ho-Baillie. Solar cell efficiency tables (version 50). *Progress in Photovoltaics: Research and Applications*, 25(7):668–676, July 2017. ISSN 10627995. doi: 10.1002/pip.2909. URL http://doi.wiley.com/10.1002/pip.2909.

[15] E. Płaczek-Popko. Top PV market solar cells 2016. *Opto-Electronics Review*, 25(2):55–64, June 2017. ISSN 12303402. doi: 10.1016/j.opelre.2017.03.002. URL http://linkinghub.elsevier.com/retrieve/pii/S1896375717300209.

[16] Jenny Nelson. *The physics of solar cells*. Imperial College Press ; Distributed by World Scientific Pub. Co, London : River Edge, NJ, 2003. ISBN 978-1-86094-340-9 978-1-86094-349-2. OCLC: ocm52689712.

[17] Montford Waltari Will. Flow of Electrons, February 2017. URL http://farhek.com/pt/92z17m/electrons-of/.

[18] A. Goetzberger and Volker U. Hoffmann. *Photovoltaic solar energy generation*. Number 112 in Springer series in optical sciences. Springer, Berlin ; New York, 2005. ISBN 978-3-540-23676-4.

[19] Purnomo Sidi, Didik Sukoco, Wahyudi Purnomo, Harry Sudibyo, and Djoko Hartanto. Electric Energy Management and Engineering in Solar Cell System. In Arturo Morales-Acevedo, editor, *Solar Cells - Research and Application Perspectives*. InTech, March 2013. ISBN 978-953-51-1003-3. doi: 10.5772/52572. URL http://www.intechopen.

com/books/solar-cells-research-and-application-perspectives/electric-energy-management-and-engineering-in-solar-cell-system.

[20] Klaus Jäger, Olindo Isabella, Arno H.M. Smets, René A.C.M.M. van Swaaij, and Miro Zeman. *Solar Energy Fundamentals, Technology, and Systems*. Delft University of Technology, 2014.

[21] Canada Mortgage and Housing Corporation (CMHC). Photovoltaic (PV) Systems, 2010. URL https://www.cmhc-schl.gc.ca/en/co/grho/grho_009.cfm.

[22] Asbjørn Skaaland, Michael Ricke, Kristin Wallevik, Rune Strandberg, and Anne Gerd Imenes. *Potential and Challenges for Building Integrated Photovoltaics in the Agder Region*. January 2011.

[23] Ionel Alboteanu, Cornelia Bulucea, and Sonia Degeratu. Estimating Solar Irradiation Absorbed by Photovoltaic Panels with Low Concentration Located in Craiova, Romania. *Sustainability*, 7(3):2644–2661, March 2015. ISSN 2071-1050. doi: 10.3390/su7032644. URL http://www.mdpi.com/2071-1050/7/3/2644/.

[24] A. N. Azmi, M. L. Kohle, and A. G. Imenes. On-grid residential development with photovoltaic systems in Southern Norway. In *2013 IEEE Conference on Clean Energy and Technology (CEAT)*, pages 93–97, November 2013. doi: 10.1109/CEAT.2013.6775606.

[25] G. H. Yordanov, T. O. Saetre, and O. M. Midtgård. 1.6 suns at 58°20N - the solar resource in Southern Norway. In *2014 IEEE 40th Photovoltaic Specialist Conference (PVSC)*, pages 0815–0820, June 2014. doi: 10.1109/PVSC.2014.6925040.

[26] Habtamu B. Madessa. Performance Analysis of Roof-mounted Photovoltaic Systems – The Case of a Norwegian Residential Building. *Energy Procedia*, 83:474–483, December 2015. ISSN 18766102. doi: 10.1016/j.egypro.2015.12.167. URL http://linkinghub.elsevier.com/retrieve/pii/S1876610215028325.

[27] Endre Barstad. Solenergiressursen i Norge. URL http://www.fornybar.no/solenergi/ressursgrunnlag/solenergiressursen-i-norge.

[28] C. Riordan and R. Hulstron. What is an air mass 1.5 spectrum? [solar cell performance calculations]. In *IEEE Conference on Photovoltaic Specialists*, pages 1085–1088 vol.2, May 1990. doi: 10.1109/PVSC.1990.111784.

[29] Furkan Dincer and Mehmet Emin Meral. Critical Factors that Affecting Efficiency of Solar Cells. *Smart Grid and Renewable Energy*, 01(01):47–50, 2010. ISSN 2151-481X, 2151-4844. doi: 10.4236/sgre.2010.11007. URL `http://www.scirp.org/journal/doi.aspx?DOI=10.4236/sgre.2010.11007`.

[30] Swapnil Dubey, Jatin Narotam Sarvaiya, and Bharath Seshadri. Temperature Dependent Photovoltaic (PV) Efficiency and Its Effect on PV Production in the World – A Review. *Energy Procedia*, 33:311–321, 2013. ISSN 18766102. doi: 10.1016/j.egypro.2013.05.072. URL `http://linkinghub.elsevier.com/retrieve/pii/S1876610213000829`.

[31] IEA. Snapshot of Global Photovoltaic Markets. Technical report, 2018.

[32] Rob W. Andrews, Andrew Pollard, and Joshua M. Pearce. The effects of snowfall on solar photovoltaic performance. *Solar Energy*, 92:84–97, June 2013. ISSN 0038092X. doi: 10.1016/j.solener.2013.02.014. URL `http://linkinghub.elsevier.com/retrieve/pii/S0038092X13000790`.

[33] Sanaz Ghazi and Kenneth Ip. The effect of weather conditions on the efficiency of PV panels in the southeast of UK. *Renewable Energy*, 69:50–59, September 2014. ISSN 09601481. doi: 10.1016/j.renene.2014.03.018. URL `http://linkinghub.elsevier.com/retrieve/pii/S096014811400161X`.

[34] Erlend Andenæs, Bjørn Petter Jelle, Kristin Ramlo, Tore Kolås, Josefine Selj, and Sean Erik Foss. The influence of snow and ice coverage on the energy generation from photovoltaic solar cells. *Solar Energy*, 159:318–328, January 2018. ISSN 0038092X. doi: 10.1016/j.solener.2017.10.078. URL `http://linkinghub.elsevier.com/retrieve/pii/S0038092X17309581`.

[35] J. C. Giddings and E. LaChapelle. Diffusion theory applied to radiant energy distribution and albedo of snow. *Journal of Geophysical Research*, 66(1):181–189, January 1961. ISSN 01480227. doi: 10.1029/JZ066i001p00181. URL `http://doi.wiley.com/10.1029/JZ066i001p00181`.

[36] A.D.J O'neill and Don M. Gray. Solar Radiation Penetration Through Snow. In *UNESCO-WMO_IAHS Symposia*, pages 227–241, College of Engineering, University of Saskatchewan, 1973.

[37] Donald K Perovich. Light reflection and transmission by a temperate snow cover. *Journal of Glaciology*, 53(181):201–210, 2007.

[38] Stephen G. Warren. Optical properties of snow. *Reviews of Geophysics*, 20 (1):67, 1982. ISSN 8755-1209. doi: 10.1029/RG020i001p00067. URL http://doi.wiley.com/10.1029/RG020i001p00067.

[39] Onni Järvinen and Matti Leppäranta. Solar radiation transfer in the surface snow layer in Dronning Maud Land, Antarctica. *Polar Science*, 7(1):1–17, March 2013. ISSN 18739652. doi: 10.1016/j.polar.2013.03.002. URL http://linkinghub.elsevier.com/retrieve/pii/S1873965213000066.

[40] Bjørn Petter Jelle, Tao Gao, Sohrab Alex Mofid, Tore Kolås, Per Martin Stenstad, and Serina Ng. Avoiding Snow and Ice Formation on Exterior Solar Cell Surfaces – A Review of Research Pathways and Opportunities. *Procedia Engineering*, 145:699–706, 2016. ISSN 18777058. doi: 10.1016/j.proeng.2016.04.084. URL http://linkinghub.elsevier.com/retrieve/pii/S1877705816300893.

[41] Iver Frimannslund. *Measurements and analysis of snow load reduction on flat roofs using a photovoltaic system in heating mode*. PhD thesis, 2017. URL https://brage.bibsys.no/xmlui/handle/11250/2464310.

[42] AgroMetBase. Hent klimadata, 2018. URL http://lmt.nibio.no/agrometbase/getweatherdata.php.

[43] Northern Alberta Institute of Technology. Solar Photovoltaic Reference Array Report. Technical report, March 2016.

[44] Gina Opstad Andersen. Preliminary study on the effect of precipitation on I-V curve characteristics. Technical report, NTNU, Trondheim, Norway, 2017.

[45] Okan Bingöl and Burçin Özkaya. Analysis and comparison of different PV array configurations under partial shading conditions. *Solar Energy*, 160:336–343, January 2018. ISSN 0038092X. doi: 10.1016/j.solener.2017.12.004. URL http://linkinghub.elsevier.com/retrieve/pii/S0038092X17310769.

[46] F. Belhachat and C. Larbes. Modeling, analysis and comparison of solar photovoltaic array configurations under partial shading conditions. *Solar Energy*, 120:399–418, October 2015. ISSN 0038092X. doi: 10.1016/j.solener.2015.07.039. URL http://linkinghub.elsevier.com/retrieve/pii/S0038092X15004107.

[47] Dmitry Baimel, Saad Tapuchi, and Nina Baimel. New Improved Maximum Power Point Tracking Algorithm for Partially Shaded PV Systems. *Journal of Power and Energy Engineering*, 05(09):55–63, 2017. ISSN 2327-588X, 2327-5901. doi: 10.4236/jpee.2017.59005. URL http://www.scirp.org/journal/doi.aspx?DOI=10.4236/jpee.2017.59005.

[48] K. Punitha, D. Devaraj, and S. Sakthivel. Artificial neural network based modified incremental conductance algorithm for maximum power point tracking in photovoltaic system under partial shading conditions. *Energy*, 62:330–340, December 2013. ISSN 03605442. doi: 10.1016/j.energy.2013.08.022. URL http://linkinghub.elsevier.com/retrieve/pii/S036054421300697X.

[49] Basim A. Alsayid, Samer Y. Alsadi, Ja'far S. Jallad, and Muhammad H. Dradi. Partial Shading of PV System Simulation with Experimental Results. *Smart Grid and Renewable Energy*, 04(06):429–435, 2013. ISSN 2151-481X, 2151-4844. doi: 10.4236/sgre.2013.46049. URL http://www.scirp.org/journal/doi.aspx?DOI=10.4236/sgre.2013.46049.

[50] Alberto Dolara, George Cristian Lazaroiu, Sonia Leva, and Giampaolo Manzolini. Experimental investigation of partial shading scenarios on PV (photovoltaic) modules. *Energy*, 55:466–475, June 2013. ISSN 03605442. doi: 10.1016/j.energy.2013.04.009. URL http://linkinghub.elsevier.com/retrieve/pii/S0360544213003095.

[51] Fei Lu, Siyu Guo, Timothy M. Walsh, and Armin G. Aberle. Improved PV Module Performance under Partial Shading Conditions. *Energy Procedia*, 33:248–255, 2013. ISSN 18766102. doi: 10.1016/j.egypro.2013.05.065. URL http://linkinghub.elsevier.com/retrieve/pii/S1876610213000751.

[52] U.S. Department of Energy. Photovoltaic Systems with Module-Level Power Electronics. Technical report, September 2015. URL https://www.nrel.gov/docs/fy15osti/64876.pdf.

[53] Nate Blair, Aron P Dobos, Janine Freeman, Ty Neises, Michael Wagner, Tom Ferguson, Paul Gilman, and Steven Janzou. System Advisor Model (SAM) General Description, January 2014. URL https://www.nrel.gov/docs/fy14osti/61019.pdf.

[54] HOMER Energy LLC. Microgrid Software for Designing Optimized Hybrid

Microgrids. URL https://www.homerenergy.com/products/pro/index.html.

[55] Eslam Allam. 7 Most Popular Solar PV Design and Simulation Software, April 2017. URL https://www.linkedin.com/pulse/7-most-popular-solar-pv-design-simulation-software-eslam-allam/.

[56] Dr. Valentin EnergieSoftware GmbH. PV*SOL® Expert Manual, January 2013. URL https://www.valentin-software.com/sites/default/files/downloads/handbuecher/en/manual-pvsol-en.pdf.

[57] PVsyst. PVsyst 5.21 Contextual Help, 2013. URL http://files.pvsyst.com/pvsyst5.pdf.

[58] European Commission. JRC Photovoltaic Geographical Information System (PVGIS) - European Commission, 2017. URL http://re.jrc.ec.europa.eu/pvgis.html.

[59] Vela Solaris AG. PolySun User Manual, 2017. URL http://www.velasolaris.com/files/tutorial_en.pdf.

[60] Petros J. Axaopoulos, Emmanouil D. Fylladitakis, and Konstantinos Gkarakis. Accuracy analysis of software for the estimation and planning of photovoltaic installations. *Int J Energy Environ Eng*, 5(1):71, April 2014. ISSN 2008-9163, 2251-6832. doi: 10.1007/s40095-014-0071-y. URL https://link.springer.com/article/10.1007/s40095-014-0071-y.

[61] Valentin Software. PV*Sol Expert: User Manual, January 2013.

[62] Lmt. URL http://lmt.nibio.no/weatherstations/43/table?from_date=15.06.2018&id=43&log_interval=1&to_date=15.06.2018.

[63] Paul W. Stackhouse. NASA Surface meteorology and Solar Energy - Available Tables. URL https://eosweb.larc.nasa.gov/cgi-bin/sse/grid.cgi?&num=191154&lat=63.47&submit=Submit&hgt=100&veg=17&sitelev=&email=&p=grid_id&p=srf_alb&step=2&lon=10.93.

[64] European Commission. JRC Photovoltaic Geographical Information System (PVGIS) - European Commission, 2018. URL http://re.jrc.ec.europa.eu/pvg_tools/en/tools.html#.

[65] Bill Marion, Robert Schaefer, Holden Caine, and Gonzalo Sanchez. Measured and modeled photovoltaic system energy losses from snow for Colorado and Wisconsin locations. *Solar Energy*, 97:112–121, November 2013. ISSN 0038092X. doi: 10.1016/j.solener.2013.07.029. URL `http://linkinghub.elsevier.com/retrieve/pii/S0038092X13003034`.

[66] J Meydbray, Keith Emery, and Sarah Kurtz. Pyranometers and Reference Cells, What's the Difference?: Preprint. *NREL*, page 7, 2012.

[67] Caroline A. Schneider, Wayne S. Rasband, and Kevin W. Eliceiri. NIH Image to ImageJ: 25 years of image analysis. *Nat. Methods*, 9(7):671–675, July 2012. ISSN 1548-7105.

[68] Ulrike Jahn, Magnus Herz, Marc Köntges, and David Parlevliet. Review on IR and EL Imaging for PV Field Applications. Technical Report 10, IEA-PVPS, 2018. URL `http://www.iea-pvps.org/index.php?id=480`.

[69] Sachin Mehta, Amar P. Azad, Saneem A. Chemmengath, Vikas Raykar, and Shivkumar Kalyanaraman. DeepSolarEye: Power Loss Prediction and Weakly Supervised Soiling Localization via Fully Convolutional Networks for Solar Panels. *arXiv:1710.03811 [cs]*, March 2018. URL `http://arxiv.org/abs/1710.03811`. arXiv: 1710.03811.

[70] H. Qasem, A. Mnatsakanyan, and P. Banda. Assessing dust on PV modules using image processing techniques. In *2016 IEEE 43rd Photovoltaic Specialists Conference (PVSC)*, pages 2066–2070, June 2016. doi: 10.1109/PVSC.2016.7749993.

[71] Peter Mark Jansson and Ulrich K. W. Schwabe. Photodiode sensor array design for photovoltaic system inter-row spacing optimization-calculating module performance during in-situ testing / simulated shading. pages 235–240. IEEE, February 2010. ISBN 978-1-4244-4988-0. doi: 10.1109/SAS.2010.5439398. URL `http://ieeexplore.ieee.org/document/5439398/`.

[72] Andrei Ilas, Pablo Ralon, Asis Rodriguez, and Michael Taylor. Renewable Power Generation Costs in 2017. Technical report, IRENA, 2018. URL `https://www.irena.org/-/media/Files/IRENA/Agency/Publication/2018/Jan/IRENA_2017_Power_Costs_2018.pdf`.

[73] Nina Jensen and Pål Ødegaard. Solkraft i Norge – Fremtidige muligheter for verdiskaping. Technical report, WWF, April 2016.

URL https://d1rirzyrd4ly69.cloudfront.net/downloads/160315_wwf_a4_screen_spread.pdf.

[74] Håkon Person. Solcellesystemer og Sol i Systemet. Technical Report 1, Solenergiklyngen, March 2018.

[75] Souhib Harb, Mohit Kedia, Haiyu Zhang, and Robert S. Balog. Microinverter and string inverter grid-connected photovoltaic system: A comprehensive study. pages 2885–2890. IEEE, June 2013. ISBN 978-1-4799-3299-3 978-1-4799-3298-6. doi: 10.1109/PVSC.2013.6745072. URL http://ieeexplore.ieee.org/document/6745072/.

[76] SunStyle. SunStyle Solar Roof Brochure, September 2017.

[77] K. Branker, M.J.M. Pathak, and J.M. Pearce. A review of solar photovoltaic levelized cost of electricity. *Renewable and Sustainable Energy Reviews*, 15(9):4470–4482, December 2011. ISSN 13640321. doi: 10.1016/j.rser.2011.07.104. URL http://linkinghub.elsevier.com/retrieve/pii/S1364032111003492.

[78] SSB. 2018-05-29. URL https://www.ssb.no/en/energi-og-industri/statistikker/elkraftpris/kvartal/2018-05-29.

[79] Vegard Holmefjord. Long-Term Market Analysis 2016. page 126.

[80] Solcellespecialisten. StecaGrid 3010x Coolcept. URL https://www.solcellespesialisten.no/inverter-vekselretter/1-fase/steca-stecagrid-3010x-coolcept.html.

[81] Solcellsgrossen. SolarEdge SE3000. URL http://www.solcellsgrossen.se/vaxelriktare/SolarEdge-vaxelriktare/solaredge-SE3000.

[82] Swedelsol. APS microinverter 500w. URL http://www.swedensol.se/produkter-solel/vaxelriktare-inverter/APS_microinverter.

[83] Yara Khawaja, Damian Giaouris, Haris Patsios, and Mohamed Dahidah. Optimal cost-based model for sizing grid-connected PV and battery energy system. pages 1–6. IEEE, October 2017. ISBN 978-1-5090-5969-0. doi: 10.1109/AEECT.2017.8257779. URL http://ieeexplore.ieee.org/document/8257779/.

[84] Solcellespesialisten and Otovo. Solkart. URL solkart.no.

Appendix A

Camera Setup and Image Processing

The following images show examples from the image processing described in this thesis.

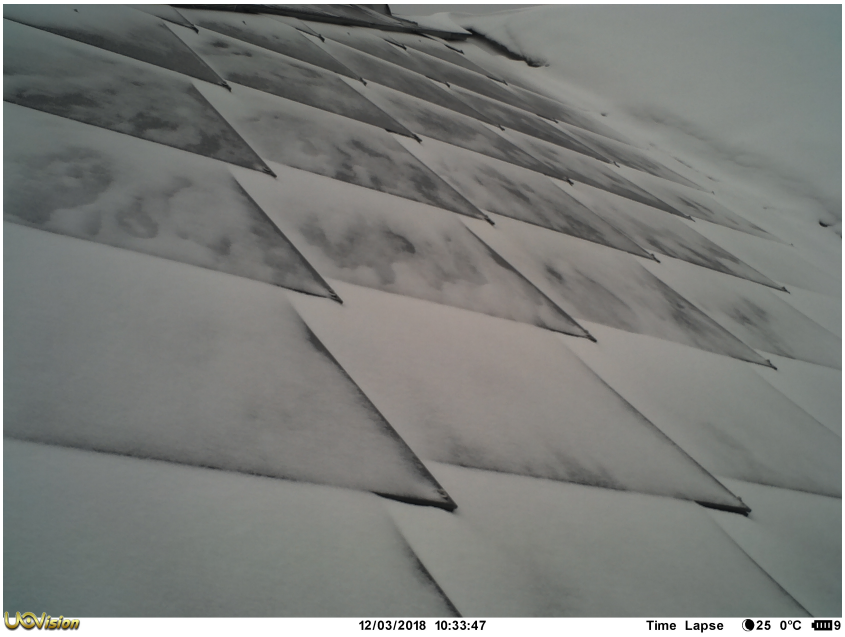

Figure A.1: Example of a time lapse image of the test site taken on 12.03.2018 at 10:33.

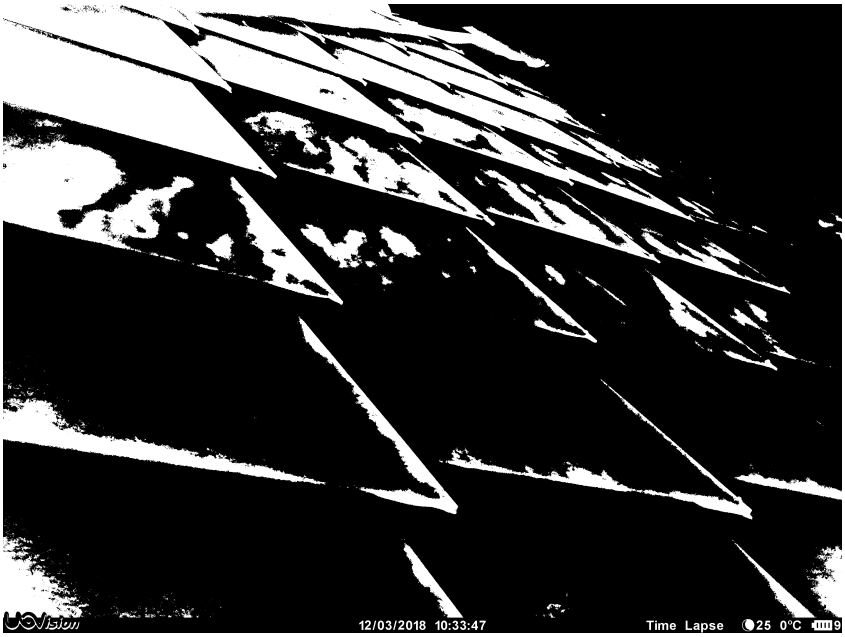

Figure A.2: Example of the result from image processing on a time lapse image of the test site taken on 12.03.2018 at 10:33.

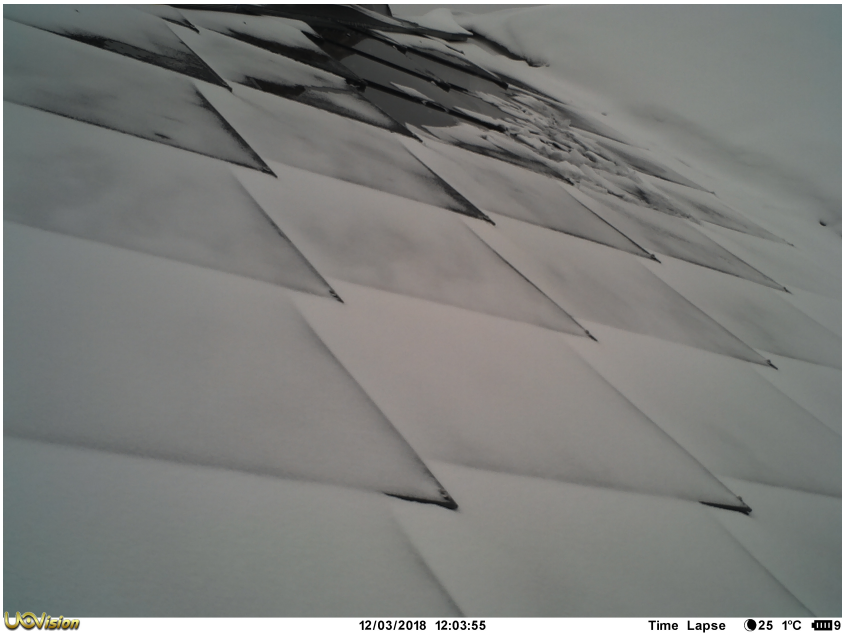

Figure A.3: Example of a time lapse image of the test site taken on 12.03.2018 at 12:03.

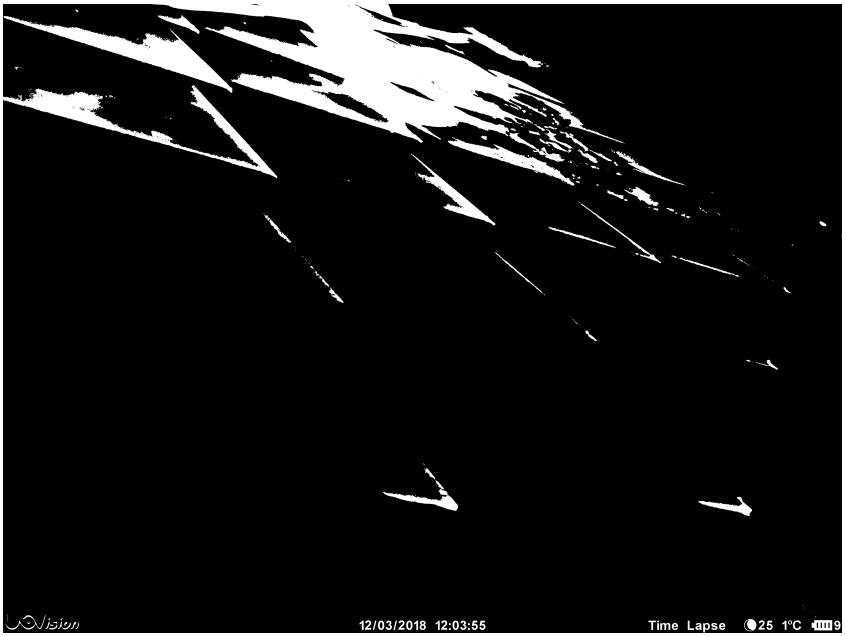

Figure A.4: Example of the result from image processing on a time lapse image of the test site taken on 12.03.2018 at 12:03.

Appendix B

System Design Drawings

The following images show documents that were used to model the 3D system in PV*Sol.

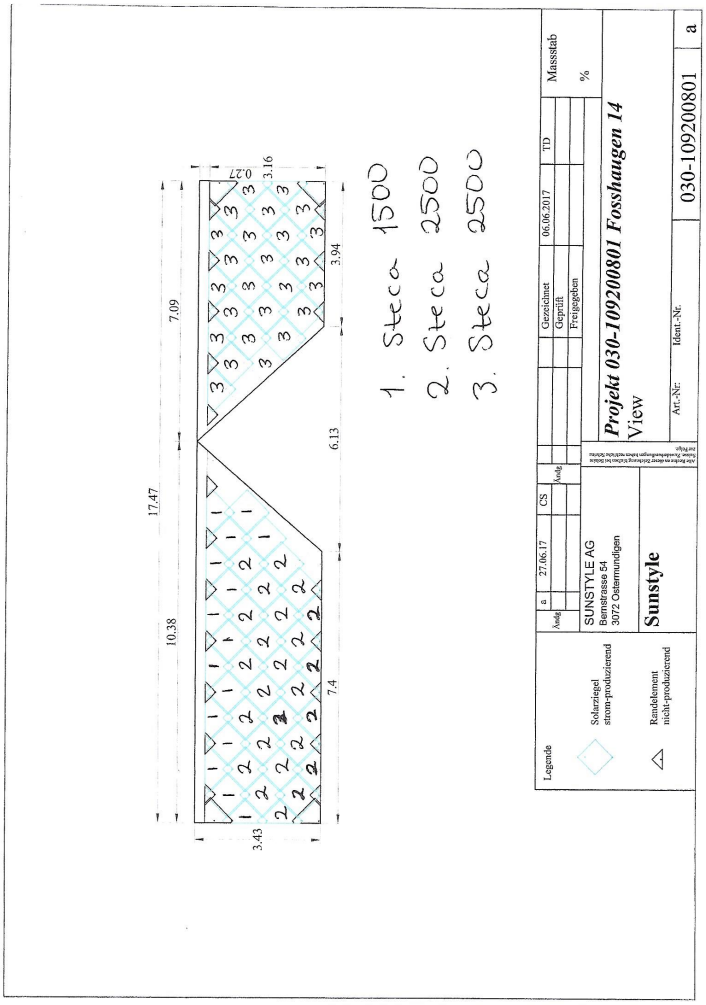

Figure B.1: Original drawings describing the module configuration where each number (1-3) represents the modules that are connected to each inverter.

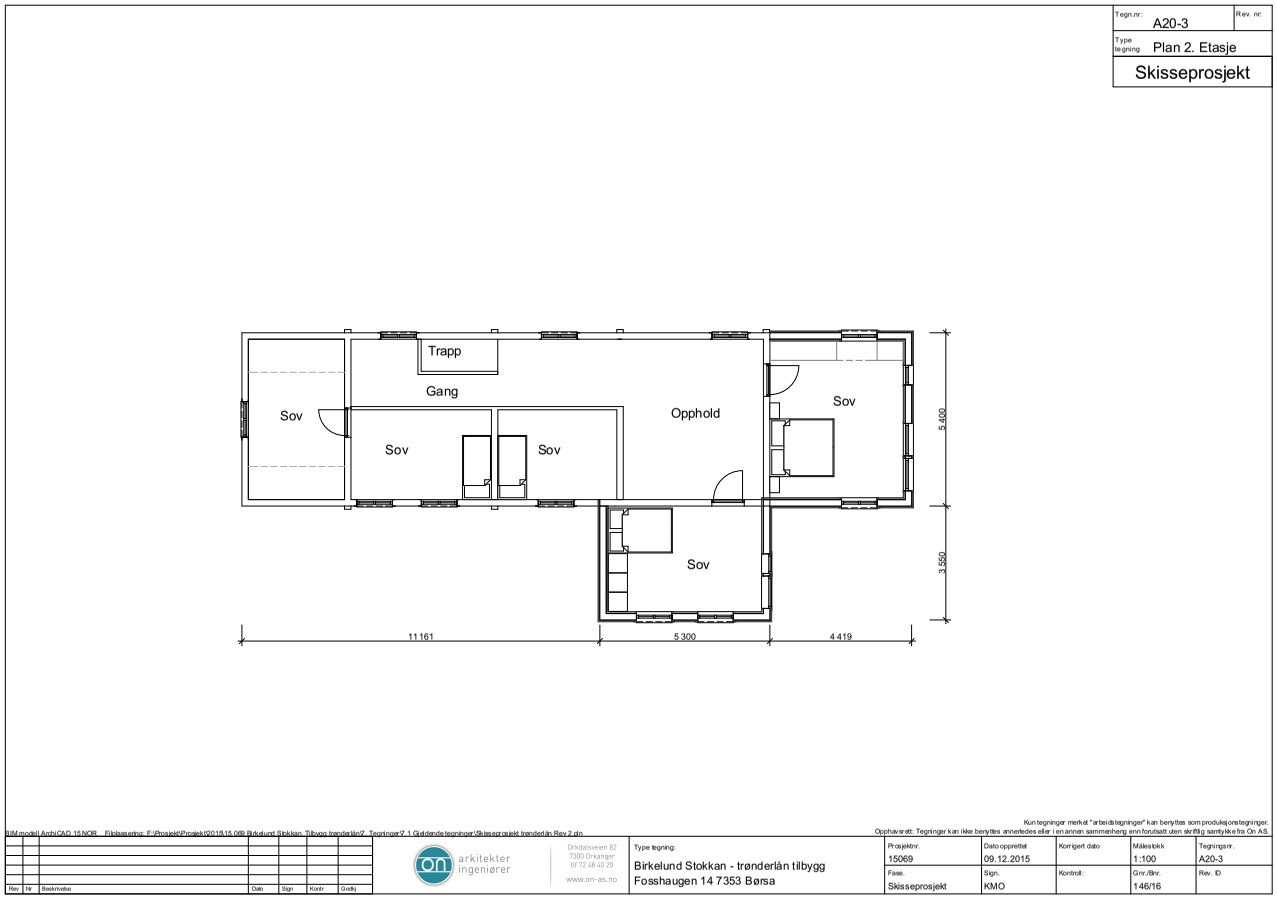

Figure B.2: Technical Drawing of house used to design 3D model in PV*Sol.

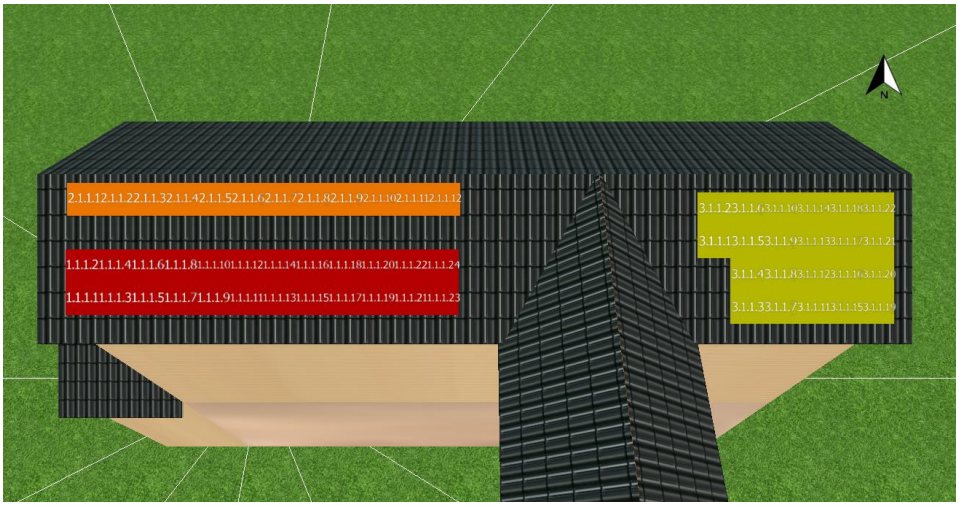

Figure B.3: Another overview of the configuration of the BIPV system with a total of 58 modules and 3 inverters. Modelled after the original plan in Figure B.1.

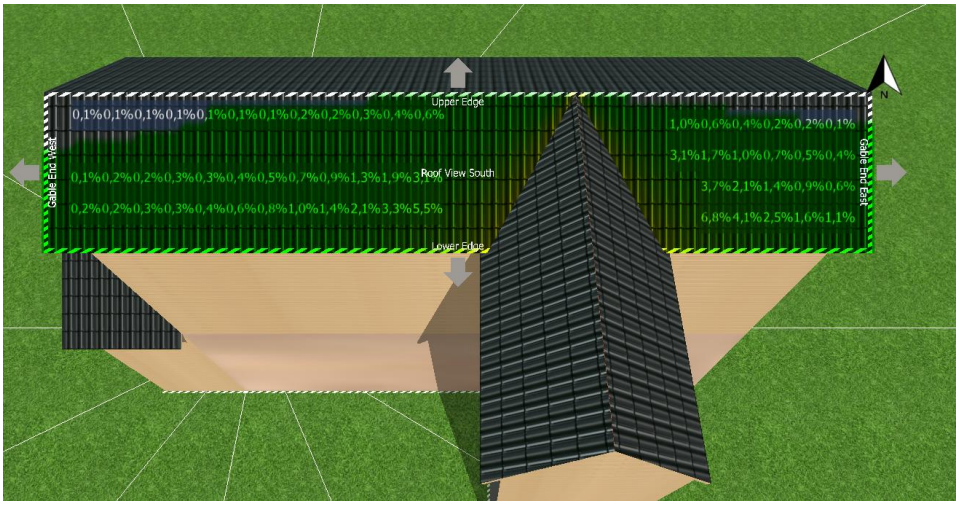

Figure B.4: The percentage of shading that each module will experience, which will affect the over performance of the system.

TECHNICAL DATA

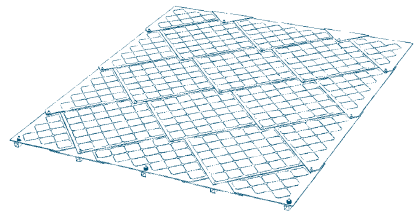

SUNSTYLE® SOLAR ROOF	
Support structure	Wood or stainless steel
Sealing elements	EPDM
Max. power per m²	155 Watt peak
Weight per m²	19,5 kg
Waterproof (tested with driving rain)	750 Pascal (136 km/h)
Wind speed (tested)	>165 km/h
Min. slope of roof	>3°

SOLAR TILES	
Material	6 mm hardened solar glass
Dimensions	870 × 870 mm
Number of solar cells	24
Solar cell type	Mono-crystalline silicon cells
Dimension of solar cells	156 × 156 mm
Max. Power (Pmpp)	100/105 Watt peak (±2,5 %)
Voltage (Vmpp)	12,5 Volt
Current (Impp)	8,4 Ampere
Open circuit voltage (Voc)	15,5 Volt
Short circuit current (Icc)	8,8 Ampere
Voltage temperature coefficient (Isc)	3,6 mA/°C
Current temperature coefficient (Voc)	-51 mV/°C
Power temperature coefficient	-0,49 %/°C

WARRANTY AND QUALITY TEST	
Product warranty	10 Years
Power warranty	90 % up to 10 Years, 80 % up to 25 Years
Quality assurance manufacturing	IEC 61730, IEC 61215, Protection Class II
Validation tests	CSTB (Scientific Technical Center for Buildings, France)
Mechanical load test	15'400 N/m² (SUPSI Swiss PV Test Center)

Figure B.5: Technical datasheet from SUNSTYLE solar roof[76].

Appendix C

PV*Sol System Inputs

The following images and documents show all inputs that were put into the PV*Sol simulation to yield the initial results.

Table C.1: Module characteristics and PV*sol inputs for the BIPV system.

Basic Data	
Company	SunStyle
Model	Solar Roof
Cell type	c-Si
Electrical Data	
Number of cells per module	24
Number of bypass diodes	Unknown (estimated 24)
Mechanical Data	
Size	870 x 870 mm
Weight	19.5 kg/m^2
IV Characteristics (at STC)	
V_{mpp}	12.5 V
I_{mpp}	8.4 A
V_{oc}	15.5 V
I_{sc}	8.8 A
FF	76.98
Nominal output	100/105 W_p ($\pm$ 2.5%)
Temperature Coefficients	
Voltage coefficient	-51 $mV/^\circ$ C
Electricity coefficient	3.6 $mA/^\circ$ C
Output coefficient	-0.49 %/$^\circ$ C
System Details	
Total size	6.2 kW_p
Number of modules	55 panels
Direction	South facing

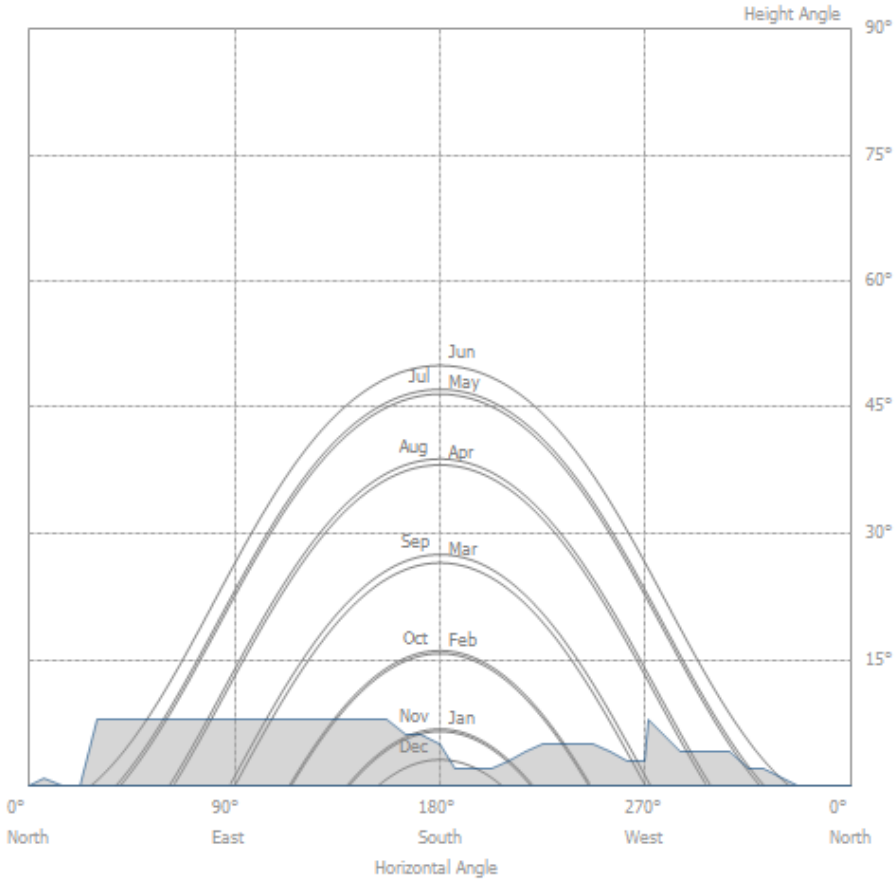

Figure C.1: Horizon profile(grey area) and monthly path of the sun (x-y axis) based on the geographical location of the test site[64].

Table C.2: Monthly ground reflection (albedo) data entered into the simulation parameters.

Month	**Surface Albedo***
January	0.20
February	0.28
March	0.31
April	0.27
May	0.20
June	0.19
July	0.13
August	0.15
September	0.14
October	0.17
November	0.22
December	0.21

*Average taken over 22 years from July 1983 - June 2005 based on a geographical boundary of 64(N) 63(S) latitude and 10(W)-11(E) longitude.[63]

Table C.3: Climate and Electrical Data Inputs from PV*Sol.

Local Climate Data	
Location	Trondheim/Værnes
Latitude	63, 47 °
Longitude	10, 93 °
Annual average temperature	6.4 ° C
Annual sum of global irradiation	866 $\mathrm{kWh/m^2}$
Local Electrical Data	
AC Voltage	230 V
Number of phases	3 phase

Appendix D

Supplementary Results

The following tables show a summary of results that were described in Chapter 6.

Table D.1: Summary of IV characteristics for 9 shading simulations.

Description	V_{oc}	I_{sc}	P_{max}	VP_{max}	IP_{max}	FF
Unshaded	37.14	8.03	224.24	29.74	7.54	0.75
A2-30 %	37.13	7.96	185.27	32.90	5.63	0.63
A2-57 %	37.28	7.98	153.68	20.39	7.54	0.52
A2-79 %	39.96	7.97	151.61	20.12	7.53	0.48
A2-79 %, C2-58 %	35.63	7.98	73.61	21.71	3.39	0.26
A2-79 %, C2-58 %, F2-30 %	36.89	5.87	77.40	22.67	3.41	0.36
Row 2 - 30 %	37.07	5.72	172.47	33.01	5.23	0.81
Row 2 - 58 %	37.03	3.45	112.34	34.40	3.27	0.88
Row 2 - 78 %	36.86	1.81	55.74	35.16	1.59	0.84

Table D.2: Inputs and assumptions used in economic assessment of inverter technologies.

Assumptions		
System size	10.92 kW_p	
Lifetime	25 years	[77]
Discount rate	4 %	[77]
Cost of electricity, 2018	0.99 NOK	[78]
Rate of inflation	4 %	[79]
Investment Costs		
String inverter	2998.95 NOK/kW_p	[80]
DC Optimizer	4265.38 NOK/kW_p	[81]
Micro inverter	4542.38 NOK/kW_p	[82]
BOS Costs		
String inverter	6293.70 NOK/kW_p	[73]
DC Optimizer	6293.70 NOK/kW_p	[83]
Micro inverter	5016.72 NOK/kW_p	[83]
Installation Costs		
String inverter	18463.28 NOK/kW_p	[84]
DC Optimizer	16616.95 NOK/kW_p	[79]
Micro inverter	14032.09 NOK/kW_p	[79]
Operations and Maintenance Costs		
All options	0.5 % of investment costs	[79]